공학박사 학위논문

The Mechanical Properties of Carbon Nanotube Yarns

탄소나노튜브 실의 역학적 특성에 대한 연구

2014년 2월

서울대학교 대학원

재료공학부

전 승 렬

The Mechanical Properties of Carbon Nanotube Yarns

Advisor: Woong-Ryeol Yu

by

Seung-Yeol Jeon

2014

Department of Materials Science and Engineering
Graduated School
Seoul National University

Abstract

Considerable efforts have been made to realize excellent material properties of carbon nanotubes(CNTs). CNT yarns have been recognized as the most attractable products derived from CNTs for their macroscopic applications. For applications to be successful, it is essential to understand the geometrical arrangement and orientation of individual CNT within CNT yarns during their deformation and the effect of such geometrical parameters on the mechanical behavior of CNT yarns. Above all, this thesis aims to predict the strength of CNT yarns.

At first, strength of CNT yarns was investigated from previous staple yarn theories based on the similarity of the geometry, i.e. individual CNTs were regarded as short fibers. From the difference between experimental and theoretical values predicted by yarn theories, it was figured out that requirement to design the strength prediction model.

The mechanical behavior of CNT yarns was investigated along with their internal changes using in-situ polarized Raman spectroscopy. Firstly, a fiber orientation function for each CNT within the CNT yarn was determined using the relationship between polarized intensities. Strain induced Raman band shifts which are related to the mechanical deformation of individual CNT within CNT yarns were investigated at concurrence. The tensile and torsional behavior of CNT yarns were then studied focusing on the motion of individual CNTs using in situ Raman spectroscopy and the existing staple yarn theory.

A new model for predicting the tensile strength of CNT yarns is developed based on their inner structure changes. To develop the model, deformation of CNT yarns was observed by using in-situ tensile test and the changes in inner structures were investigated by focused ion beam milling process. Based on the experimental results, failure mechanism was defined and theoretical model was built up in respect of interfacial shear stress originated from Van der Waals forces and frictional stresses due to the lateral pressure generated from inherent yarn structure. A new concept, CNT clusters which divides CNT bundles like as unit cell and have hexagonal packed structure was introduced to define the model. With the ‘CNT cluster’ concept accepted, the strength of

CNT yarns was predicted by combine interfacial shear stress and frictional stress. The prediction is then compared with experiments to validate that the current model incorporating the CNT cluster is highly suitable for predicting the tensile strength of CNT yarns.

Finally, strategy for enhancing the strength of CNT yarns was suggested based on the results of this study.

Keywords: Carbon nanotube yarns, tensile strength, mechanical behavior, Raman spectroscopy, molecular dynamics, interfacial shear stress

Student Number: 2008-20679

Contents

List of Figures

List of Tables

Chapter 1. Introduction

1.1 Carbon nanotube yarns

Carbon nanotubes(CNTs) have excellent material properties such as high electrical conductivity, thermal conductivity and mechanical properties. The electrical resistivity of single-walled nanotubes(SWNTs) and of multi-walled nanotubes(MWNTs) were measured as low as $10^{-6}\Omega m$ and $3 \times 10^{-6}\Omega m$, respectively[1-4]. SWNT has thermal conductivity along its axis about 3500W/mK at room temperature[5]. In case of MWNTs, the observed thermal conductivity is more than 3000W/mK[6]. Young's modulus of SWNTs and MWNTs were observed as ~1TPa and tensile strength of them was measured as 10~150GPa, respectively[7-9]. However, it is not easy to handle them and realize their nanoscale properties in macro scale. Thus, CNTs have been processed to yarns via textile technologies, aiming to utilize their remarkable mechanical and electrical properties in micro/macro scales.

CNT yarn manufacturing processes are divided into two types, wet spinning method and dry spinning method. Wet spinning which is similar to the coagulation spinning fabricating conventional polymer fibers is the method of using surfactant-stabilized CNT dispersion solution. The dispersion system is destroyed by amphiphilic polymer solution such as polyvinylalcohol(PVA) and various acids(hydrochloric, sulfuric, nitric, and phosphoric) or bases(NaOH and KOH), since they partially replace surfactant which surround a CNT so that CNTs are aggregated. While CNT agglomeration

creates, the form of a fiber is produced by inducing liquid flow. In case of fibers using wet spinning methods, however, it results in fibers with low electrical and thermal conductivity, since most of polymers are non-conductive. Furthermore, removal a large amount of polymer is not easy task without maintenance fiber feature. From the polymer-free processes using acids or bases, pure CNT fibers could be obtained, however the chemical dispersing process leads to a low usage of CNTs and induces residual contamination of CNTs from the fluid. The resulting neat fiber has mechanical and physical properties much lower than individual CNTs, thus dry spinning methods were suggested as alternatives. By using the chemical vapor deposition(CVD) methods with a floating catalyst, CNT yarns could be obtained by spinning directly from the CVD synthesis zone of a furnace. In addition, SWCNT fibers by twisting SWCNT films prepared by a floating catalyst CVD. Meanwhile, CNT yarns could be produced by spinning from vertically aligned CNT arrays.

Although several efforts have been performed to produce CNT yarns, their physical properties are still much lower than individual CNTs[10-13]. Thermal and electrical conductivity of CNT yarns are in the order of 100W/mK and 100S/cm which are one order less than them of CNTs. In the case of mechanical properties, there are significant differences compared to other properties. CNTs possess superb mechanical properties including elastic modulus and strength, ~1TPa and ~50GPa for multi-walled nanotubes, respectively, while modulus and strength of CNT yarns are in the order of 10GPa and 1GPa. Therefore, theoretical studies are needed to investigate the reason why CNT yarns have such lower physical properties. In this study, we

focused on the strength of CNT yarns based on their inner structure.

1.2 Theoretical studies on the strength of carbon nanotube yarns

Theoretical analysis of the strength of CNT yarns have been performed by several research groups. The relationship between Weibull strength CNTs and the statistical failure behavior of CNT yarns was demonstrated by Beyerlein et al.[14]. The statistical strength with surface twist angle, number of CNTs in cross-section, and gauge length were predicted using Monte Carlo simulation. Vilatela et al.[15] investigated deformation of CNT bundles by concentrating on stress transfer mechanism based on the interfacial shear stress between CNTs. CNT fiber strength were determined according to the nanotube length, shear strength and contract area between CNTs. The interactions among CNTs in a yarn examined by Lu et al.[16] They established the model regarding CNT entanglement as two connecting self-folded CNTs originated from the van der Waals interactions. It was demonstrated that tensile properties of CNT entanglements with geometrical condition such as CNT radius and length. Meanwihle, The deformation and strength mechanism was investigated by using coarse-grained molecular dynamics simulations[17]. The fully atomistic CNT model was replaced by a line of beads connected via springs and van der Waals forces between the beads were considered. Stress–strain relationships of CNT fibers with failure mechanism were determined with the structural evolution mechanisms of CNT fibers under tension.

Although various models to predict mechanical properties were established as stated above, mechanical properties of CNT yarns developed in recent years is still lower compared to individual CNTs. Existing models supposed the geometry of CNT yarns treated in classical yarn theory, i.e. idealized helical yarn structure. In other words, there was lack of the consideration on the actual geometry of CNT yarns. In addition, CNT agglomerations could be created inside the yarn when gaps between CNTs become shorter than Van der Waals length(about 3.4Å). It is possible that the existence of agglomerations make CNT yarns non-uniform, thus, a new model should be needed to consider them.

1.3 Research objectives

In this thesis, the main objective is to develop the model predicting strength of the CNT yarns and suggest a strategic method for significantly enhancing the mechanical properties of CNT yarns.

In the chapter 2, the strength of CNT yarns was investigated from two previous yarn theories. One is a statistical approach based on the weakest link theory of single fiber, i.e. the strength of single fiber is characterized by Weibull statistics. The other is a mechanical approach, theory of the mechanics of staple fiber yarns. Assuming the idealized helical structure composed of a series of concentric cylinders of differing radii and uniformly distributed perfect elastic fibers, force equilibrium on the fiber element was calculated. Finally, problems of the existing staple yarn theories were analyzed from the discrepancy between theoretical value and experimental

value.

In the chapter 3, the mechanical behavior of CNT yarns, which were manufactured by twisting CNT sheets drawn from CNT forests, was investigated along with their internal changes using in-situ Raman spectroscopy. Firstly, a fiber orientation function for each CNT within the CNT yarn was determined using Raman bend shifts, which are related to the mechanical deformation of individual CNT within CNT yarns. The tensile and torsional behavior of CNT yarns were then studied focusing on the motion of individual CNTs using in situ Raman spectroscopy and the existing staple yarn theory.

In the chapter 4, to predict the tensile strength of CNT yarns, deformation of CNT yarns was observed by using in-situ tensile test and the changes in inner structures were investigated by FIB milling process. Based on the experimental results and the knowledge obtained from chapter 3, failure mechanism was defined and theoretical model was built up in respect of interfacial shear stress originated from Van der Waals forces and frictional stresses due to the lateral pressure generated from inherent yarn structure. A new concept, CNT clusters which divides CNT bundles like as unit cell and have hexagonal packed structure was introduced to define the model. Assuming that close packing of circular CNTs in hexagonal outline only effect on the interfacial shear stress, the effect of Van der Waals forces was considered in the model. Meanwhile, classical yarn theory was adopted to investigate the structure effect of the yarn. The influence of the number of CNT cluster which reflects the inner structure of CNT bundle and radial

position in which fracture occurs on tensile strength was investigated. Finally, the method to improve tensile strength was proposed based on theoretical model.

Chapter 2. Theoretical prediction based on existing yarn theories

2.1 Introduction

Carbon nanotubes(CNTs) have excellent material properties such as high electrical conductivity, thermal conductivity and mechanical properties. However, it was not easy to handle them and realize their properties without loss in macro scale, thus they should be assembled to utilize their properties. In this respect, CNTs have been processed to yarns, bundles and textile structures based on them by imitating textile spinning technology for the purpose of utilizing their remarkable mechanical and electrical properties in micro/macro scales in recent years[18-21]. The mechanical properties of yarns, such as tensile modulus and strength, influence strongly the mechanical performance of such textiles, thus are important factors to be predicted. As such the mechanical modeling of yarns in the macro and micro scale has been researched in the textile community. It is, however, uncertain that existing yarn theories can be used to predict the mechanical properties of CNT yarns due to their nanoscale constituents(CNTs).

CNT yarns as a micro-fiber structure consists of nanoscale CNTs has been manufactured modifying conventional fiber engineering. Manufacturing methods of CNT yarns depending on the way they are spun is divided into two significant ways, wet spinning and dry spinning. Wet spinning modified by the coagulation spinning fabricating conventional polymer fibers is the

method of using CNT dispersion solution[22-24]. However the chemical dispersing process leads to a low usage of CNTs and induces residual contamination of CNTs from the fluid. The resulting neat fiber has mechanical and physical properties much lower than individual CNTs, thus dry spinning methods were suggested as alternatives. Dry spinning processes are classified into two major methods. One is directly synthesis method using floating catalytic chemical vapor deposition method(FCCVD)[25, 26]. The other is a method of manufacturing from a set of long vertically aligned CNTs, such as CNT forest. Drawing carbon nanotubes from a CNT forest, a simple way to create a continuous yarn, has been studied[12, 27]. However, the properties of CNT yarns fabricated by the process fall significantly behind CNT itself. In case of mechanical properties, for example, CNT yarns with a tensile strength significantly decreases at 150 ~ 1GPa much lower than strength of CNT[9, 28, 29].

In this chapter, strength of CNT yarns was investigated from two previous yarn theories. One is a statistical approach based on the weakest link theory of single fiber, i.e. the strength of single fiber is characterized by Weibull statistics[30]. According to the approach, the strength of twisted yarns was determined by the breakage probability of the single fiber considering the effects of inter-fiber friction during yarn extension. The other is a mechanical approach, theory of the mechanics of staple fiber yarns[31]. Assuming the idealized helical structure composed of a series of concentric cylinders of differing radii and uniformly distributed perfect elastic fibers, force equilibrium on the fiber element was calculated. For the calculation, some parameters such as Young's modulus of CNT, frictional coefficient

between CNTs and Weibull parameters representing stochastic strength of CNTs were cited from several literatures.

2.2 Statistical approach

Prediction of statistical strength of the short fiber yarns which was introduced by Pan[30] is based on Daniel's model for a parallel fiber bundle. The yarn was regarded as a chain of fiber bundles and the structural parameters such as orientation angle of constituent fibers in accordance with twisted fiber structure and volume fraction were considered to the model. In addition, the effects of inter-fiber friction was introduced using critical length concept. In this model, there are certain assumptions. First, the fiber helix angles are uniformly distributed from zero to the value at the yarn surface without considering the fiber migration(Fibers which are on the surface at one point along the yarn must be inside the yarn at other points). Next, fiber strength is according to the Weilbull distribution and stress concentration is ignored. The theory behind the model is discussed briefly in the following paragraphs.

2.2.1 Stress transfer between constituent fibers in short fiber yarns

The tensile behavior of short fiber yarns is determined by the stress applied to the constituent fibers, which are transferred by the friction between fibers. Such stress transfer can be explained by using a short-fiber composite model (shear lag theory)[32] that assumes a fiber (reinforcement) surrounding or neighboring other fibers (matrix)(see Figure 2-1).

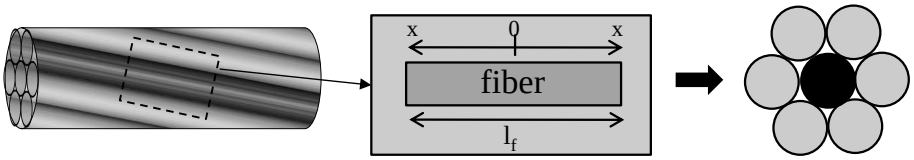

Figure 2-1. Load transfer from a fiber to neighboring fibers in the short fiber yarn.

The fiber tensile stress is obtained using the shear lag theory as follows:

$$\sigma_f = E_f \varepsilon_f \left[1 - \frac{\cosh(ns / r_f)}{\cosh(ns)} \right] \quad (1)$$

where E_f and r_f represent the tensile modulus and radius of the fiber, respectively. Note that n is the value indicating the cohesion among fibers [30] given by,

$$n = \sqrt{\frac{G_{TL}}{E_f} \frac{2}{\ln 2}} \quad (2)$$

where G_{TL} is the longitudinal shear modulus of the nonwoven, which can be calculated using the fiber modulus, the fiber volume fraction and orientation and the length efficiency factor defined from shear lag theory [32]. s is the aspect ratio (fiber length divided by its diameter). The averaged tensile stress throughout the fiber can be calculated by integrating

Equation 2 over l_f, and can be expressed by:

$$\overline{\sigma_{fl}} = \left(1 - \frac{\tanh(ns)}{ns}\right) E_f \varepsilon_f = \varsigma E_f \varepsilon_f \qquad (3)$$

where ζ is the fiber length efficiency factor. As this factor approaches value 1, it implies that uniform stress will be developed in the whole fiber, i.e. perfect stress transfer between fibers. The shear stress can be derived noting that the maximum shear stress occurs at the fiber ends.

$$\tau = \left(\frac{nE_f \varepsilon_f}{2} \frac{\sinh(nx/r_f)}{\cosh(ns)}\right) \qquad (4)$$

Then, the lateral pressure (g) between fibers is defined by a linear relationship with the shear stress value via a frictional coefficient($\tau = \mu g$).

2.2.2 The statistical strength of short fiber yarns

According to the weakest link theory[33], the probability of the fiber breakage against the tensile stress(σ) is

$$F(\sigma) = 1 - \exp(-l_f \alpha \sigma^{\beta}) \qquad (5)$$

where α and β are Weibull parameters which are the scale parameter and the shape parameter, respectively. Weibull parameters are independent of the fiber length, l_f. The expected value of the fiber strength is

$$< \sigma_f >= \int \sigma F(\sigma) d\sigma = (l_f \alpha)^{-1/\beta} \Gamma\left(1 + \frac{1}{\beta}\right) \qquad (6)$$

Assuming that when a fiber breaks, the load is equally distributed among all unbroken fibers. Then Daniel's statistical model[34] for parallel fiber bundle made of a very large number of fibers is predicted as followings.

$$< \sigma_b >= (l_f \alpha\beta)^{-1/\beta} \exp\left(-\frac{1}{\beta}\right) \tag{7}$$

Pan[30] developed a statistical model to predict the tensile strength of staple yarns modifying equation 7.

$$\sigma_f = \eta_q V_f (l_c \alpha\beta)^{-1/\beta} \exp\left(-\frac{1}{\beta}\right) \tag{8}$$

Here η_q is the orientation efficient factor given by:

$$\eta_q = \frac{2q(1-\nu_{LT}) + (1+\nu_{LT})\sin 2q}{4q} \tag{9}$$

Where ν_{LT} is the Poisson's ratio of a nonwoven mat, which can be also calculated using a theoretical equation from [35]. q is the fiber orientation angle. V_f is fiber volume fraction. l_c in Equation 8 is the critical length given by Kelly and MacMillan [36]:

$$l_c = \frac{r_f \sigma_{fb}}{\tau} \tag{10}$$

where σ_{fb} and τ are the fiber strength (dependent on the fiber length) and the interfacial shear strength, respectively. Note that l_c was rewritten for the staple yarn theory using the lateral pressure (g) between fibers and

the frictional coefficient (μ) as follows:

$$l_c = \frac{r_f \sigma_{fb}}{\tau} = \left(\frac{r_f \sigma_{fb}}{\mu g} \right) \quad (11)$$

Then, the following equation was derived:

$$l_c = \left(\frac{2 r_f \sigma_{fb}}{n E_f \varepsilon_f \tanh(ns)} \right) \quad (12)$$

The tensile strength of nonwoven mats was then defined using Equation 8 and its necessary parameters, which will be determined by experiment and by citing data from existing literatures as follows.

2.2.3 Prediction of the tensile strength of CNT yarns

For calculation of statistical strength of a CNT yarn, necessary parameters in equation 8 should be determined in accordance with the characteristics of individual CNTs and interfacial properties of them. At first, CNT yarns were fabricated and structural parameters such as yarn helix angle(q) and volume fraction(V_f) were measured. Yarn helix angle was simply measured as 31.11° by observing surface of the yarn using scanning electron microscope(SEM, JEOL JSM-6390LV). For measurement of volume fraction, density of CNT yarn was determined by weighing a 300mm length of yarn sample on a Mettler Toledo AX26DR Ultra Micro Balance and dividing yarn volume. Volume fraction of CNT yarns was calculated by dividing nanotube density of 2.1/cm^3[37]. In this case, volume fraction was measured as 0.3201. Meanwhile, Barber et al.[38] examined Weibull parameters summarizing experimental data for the tensile strength of

individual nanotubes of any sort(see Table 1).

Table 1. Weibull shape and scale parameters of the strength distributions of the CNTs[38].

Nanotube material	$\alpha(m^{-1}GPa^{-1})$	B	Nanotube strength(GPa)
CVD carbon MWNTs(GL:10±4μm)	34.2	1.7	80~132
AD carbon MWNTs(GL:1~11μm)	42.3	2.4	21.68~58.89
WS_2 carbon MWNTs(GL:2~5μm)	6.34E-4	7.7	11.93~13.44

CVD carbon MWNTs are produced by chemical vapor deposition(CVD) and AD carbon MWNTs are grown by the arc-discharge method. WS_2 carbon MWNTs are nanotubes which structure is composed in the form of closed polyhedral and cylindrical crystals of tungsten disulphide(WS_2) and produced by the fluidized bed reactor method[39]. According to Weibull parameters, nanotube strength depending on the nanotube length is calculated using equation 6(see Figure 2-2-2).

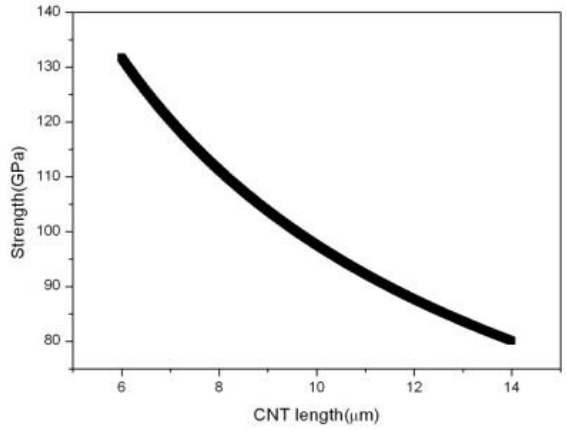
Strength(GPa)
CNT length(μm)
140
130
120
110
100
90
80
6
8
10
12
14

(a)

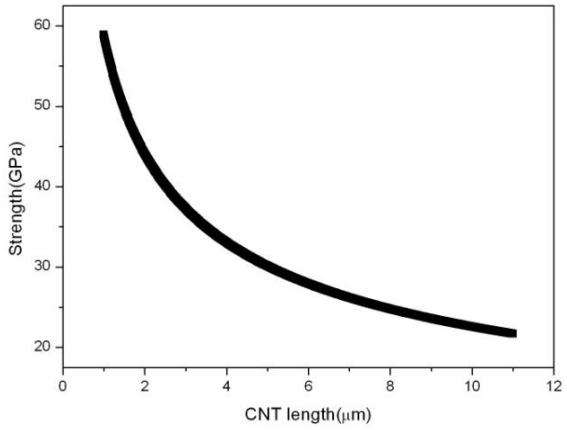
Strength(GPa)
CNT length(μm)
60
50
40
30
20
0
2
4
6
8
10
12

(b)

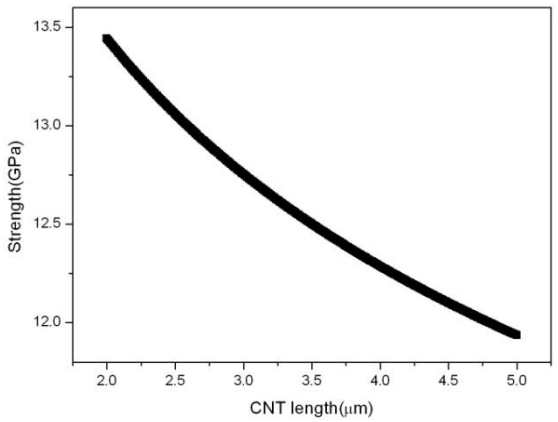

(c)

Figure 2-2. Strength of various type of nanotubes depending on the nanotube length. (a) CVD carbon MWNTs, (b) AD carbon MWNTs, (c) WS_2 carbon MWNTs.

Indeed, Weibull parameters reflect the regularity of nanotube structure. Shape parameter, β indicates a variability in tensile strength, i.e. characterizes the spread of the strength. As β increases, the nanotube has more regular wall structure. In other words, nanotubes which have low value of β reflect the large tube defect density. Thus, the tensile strength of CNTs produced by CVD is distributed more widely than AD carbon CNTs and WS_2 carbon CNTs. In classical Weibull model, β has another physical meaning. The more brittle material, the lower the value of β. Indeed, carbon fibers which have graphitic structure have smaller values of β as the fiber modulus increases. Meanwhile, scale parameter, α is closely related with the mean of the strength. By multiplying average length for each

nanotube to α (simply multiplying 10μm, 5.5μm and 3.5μm for CVD carbon MWNTs, AD carbon MWNTs and WS_2 carbon MWNTs, respectively), CVD carbon CNTs have highest strength although they have larger defects than other CNTs. This phenomenon was explained focusing on the inter-tube stress transfer[40]. CNTs composed of well-ordered walls tend to cause slippage between walls when they are strained, while inter-wall interaction increases in CNTs with irregular multi-wall structure. Thus, contradictively, larger absolute forces are required to fracture more irregular nanotubes despite of a large variation in the tensile strength.

Finally, critical length(l_c) was determined by calculating lateral pressure between CNTs inside CNT yarn. A structural mechanics approach was developed and used to calculate the mechanical behavior of CNTs[41]. Structural mechanics considering the potential function in molecular dynamics(MD) can be an alternative option because it can readily incorporate the properties of CNTs into continuum scale structure and their mechanical behavior can be calculated using well established methods such as finite element method. Here, the mechanical properties of CNTs are important in this approach and can be determined using MD simulation. In this research the following mechanical properties were used for each CNT which diameter set as 10nm(Table 2.[41]).

Table 2. Mechanical properties of CNTs(diameter:10nm) for structural mechanics approach.

Modulus(Young's) [GPa]	Poisson ratio
E_1: 113 E_2: 113 E_3: 1130 G_{12}: 44.6 G_{13}: 470 G_{23}: 470	ν_{12}:0.267 ν_{13}:0.048 ν_{23}:0.048

Then, a finite element model was constructed by modeling each CNT inside CNT yarns using a 3-dimensional element and used to determine lateral pressure(g) in equation 11. A geometric model for CNT yarn was constructed as shown in Figure 2-3.

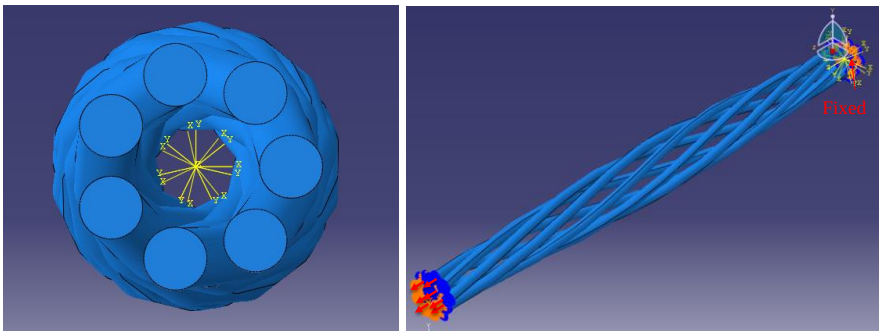

(a) (b)

Figure 2-3. CNT yarn model with close-packed structure (a) and the boundary conditions for twisting operation (b).

A twisting operation was then simulated by imposing the fixed boundary condition on the bottom side of each CNT, while its top side was tensioned parallel to the yarn axis. Seven CNTs were used in the modeling assuming the hexagonal close-packed structure of CNTs inside yarn. The finite element analysis was carried out to calculate the lateral pressure between CNTs inside the yarn according to tension applied to each CNT. Van der Waals interaction, which was calculated by Lennard-Jones potential between CNTs(see Figure 2-4), was included in addition to the frictional force during the lateral pressure calculation.

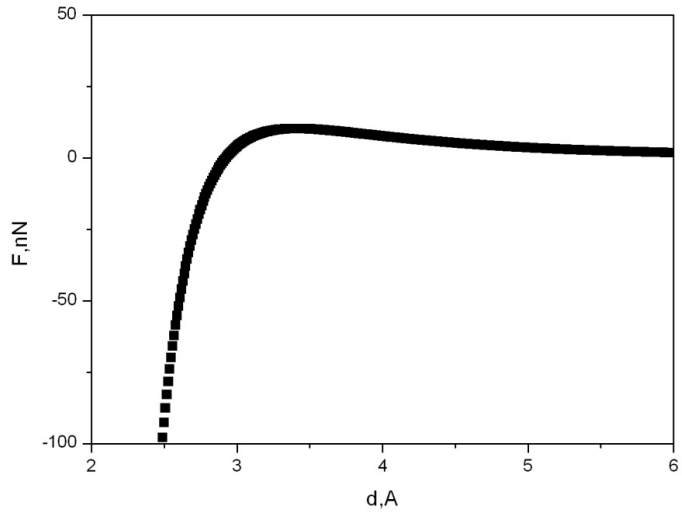

Figure 2-4. Van der Waals forces between two identical CNTs (diameter:10nm).

The lateral pressure was calculated using finite element analysis(see Figure 2-5). The maximum lateral pressure (3.57GPa) was calculated when the stress (13.84GPa) was applied to each CNT. The frictional coefficient of CNTs(μ) is generally determined by their arrangements[42]. When CNTs were vertically aligned, the frictional coefficient was found to be about 0.9. This value was adopted in this study. Due to the high friction and the CNT migration in the yarn, the yarn interior is not hexagonal close packed structure. Geometric irregularities within CNT yarn exist and may reduce lateral pressure than hexagonal close packed case, which can again lower the mechanical properties of CNT yarns. Then critical length(l_c) was calculated as 43.14nm using equation 11.

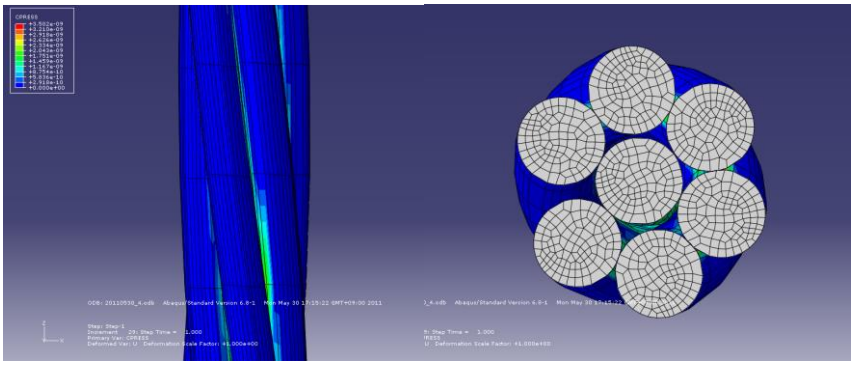

(a) (b)

Figure 2-5. Twisted and deformed shape of CNT yarn (a) and its cross section (b).

Based on the calculated parameters, the statistical strength of CNT yarns for various types of individual CNTs was predicted as Table 3.

Table 3. The statistical strength of CNT yarns

Nanotube material	$\alpha(m^{-1}GPa^{-1})$	B	Yarn strength(GPa)
CVD carbon MWNTs(GL:10±4μm)	34.2	1.7	53.71~72.01
AD carbon MWNTs(GL:1~11μm)	42.3	2.4	5.75~8.72
WS_2 carbon MWNTs(GL:2~5μm)	6.34E-4	7.7	0.47~0.48

Note that variation of the strength is depended on the shape parameter(β), i.e. the strength distribution is inversely proportional to β, thus the strength of CVD carbon MWNTs is relatively widely distributed. Comparing with the strength of individual CNTs, CNT yarns have strength ranges from between 3.57%(WS_2 carbon MWNTs) and 67.14%(CVD carbon MWNTs) of individual CNTs according to Weibull parameters. CNT yarns treated in this study was consisted of CNTs produced by CVD. To validate strength prediction, the tensile strength of CNT yarns was measured using a single-fiber tensile test following the ASTM D3822-07 specification(see Figure 2-6). Gauge length of CNT yarns was 10mm and strain rate set as 1mm/min.

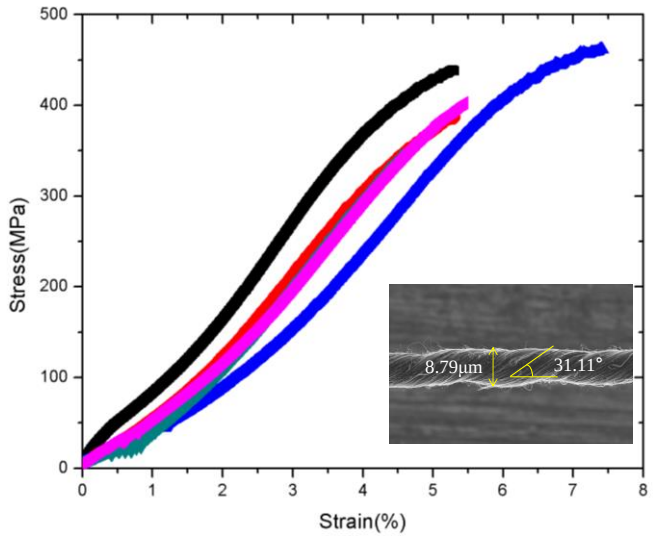

Figure 2-6. Stress-strain curve of CNT yarns. The inset figure represents a geometry of CNT yarns measured in the tensile test.

The average tensile strength was measured as 394.14MPa with standard variation, 42.51MPa and average failure strain was measured as 5.64% with standard variation, 1.04. The predicted value is much higher than experimental values, i.e. the actual measurement is two orders of magnitude lower than we predicted. First, the discrepancy can be explained by the modeling approach (the current geometry for calculating critical length is closed to filament yarn). In case of short-fiber yarns, slippage occurs at the end of fiber, thus greater lateral pressure was calculated without consideration of slippage. Furthermore, the experimental values we compared were obtained from CNT yarns produced by a dry method (a spinning process from aligned CNT arrays). The inner structure of CNT

yarns created by this process is composed of a core-sheath structure[43]. Packing density becomes higher from the sheath to the core due to the existence of lateral pressure of the yarn. Due to Van der Waals interaction between CNTs, CNTs agglomerate together to form bundle and degree of bundling depends on the packing density. Thus, individual CNTs cannot carry external forces equally and it does not agree with the assumption in bundle theory. In addition, some constituent CNTs in CNT yarns are not straight but crimped. Crimped CNTs does not receive external force perfectly until they are stretched, thus the existence of crimped CNTs should be taken into account in the model. Moreover, misalignment of CNTs will decrease the stresses in CNTs within the yarn due to the obliquity effect. Volume fraction is also an important parameter to determine the strength. The yarn geometry is not exactly a cylinder, thus it is possible that the volume fraction was measured larger than real value. As a result, the actual strength of CNT yarns was lower than their theoretical value.

2.3 Mechanical approach

2.3.1 The theory of the mechanics of short fiber yarns

The theory of the mechanics of staple fiber yarns was introduced by Hearle[31]. For a given external force, the response of a structure such as the resultant deformation, the internal stresses and strains is calculated. The strength calculation starts from taking into account relationship between individual fiber extension and yarn extension. Considering yarn geometry which have the idealized helical structure, the relationship is calculated as followings(see Figure 2-7).

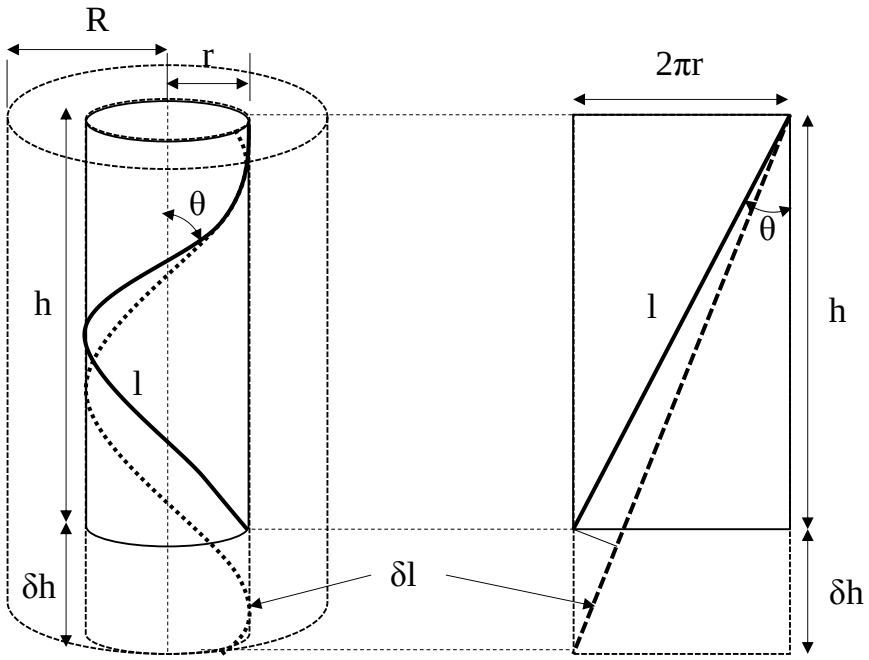

Figure 2-7. Geometry of yarn subject to tensile force[31].

The quantities *R*, *r*, *h*, θ and *l* are yarn radius, radius of cylinder containing the helical path of a particular fiber, yarn length of one turn of twist, helix angle at radius *r* and fiber length of one turn of twist at radius *r*, respectively. Assuming no change in yarn diameter during extension, yarn extension is

$$\varepsilon_y = \delta h / h \tag{13}$$

and there is a relationship.

$$l^2 = h^2 + 4\pi^2 r^2 \tag{14}$$

The variation of strain through the yarn is given by differentiating the relationship

$$2ldl = 2hdh + 8\pi^2 rdr \tag{15}$$

and

$$\frac{dl}{l} = \frac{h^2}{l^2}\frac{dh}{h} - \frac{4\pi^2 r^2}{l^2}\nu_{LT(yarn)}\frac{dh}{h} \tag{16}$$

where $\nu_{LT(yarn)}$ is Poisson's ratio of yarn

Then, fiber extension is

$$\varepsilon_f = \frac{\delta l}{l} = \varepsilon_y\left(\cos^2\theta - \nu_{LT(yarn)}\sin^2\theta\right) = \varepsilon_y\left(\frac{c^2}{u^2} - \nu_{LT(yarn)}\left(1 - \frac{c^2}{u^2}\right)\right)$$
$$u = l/L \tag{17}$$
$$c = \cos\alpha = h/L$$

where L and α are length of fiber in one turn of twist and surface angle at radius R(yarn radius), respectively.

Using the correlation between fiber and yarn strain, stress-strain relation is determined assuming that the fiber extension follows Hooke's law as followings

$$\varepsilon_f = \frac{\sigma}{E_f} - \frac{2\nu_{TL}}{E_f'}(-G) \tag{18}$$

where σ, E_f, E_f', ν_{TL} and G are a tensile stress applied to the fiber, tensile modulus of fiber, transverse modulus of fiber, transverse Poisson's ratio of fiber and compressive transverse stresses. The fiber has axis-symmetry, thus

$$\varepsilon_f = \frac{\sigma}{E_f} - \frac{2\nu_{LT}}{E_f}(-G) \tag{19}$$

where ν_{LT} is axial Poisson's ratio of fiber.

Combining equation 17 and 19, stress-strain relation of the fiber is represented as

$$\sigma = E_f \varepsilon_f \left[\frac{c^2}{u^2} - \nu_{LT(yarn)} \left(1 - \frac{c^2}{u^2} \right) \right] - 2\nu_{LT} G \tag{20}$$

Meanwhile, radial equilibrium(the net forces acting on the yarn element in the direction of the yarn radius is zero) should be considered to compressive transverse stress(G)(see Figure 2-8).

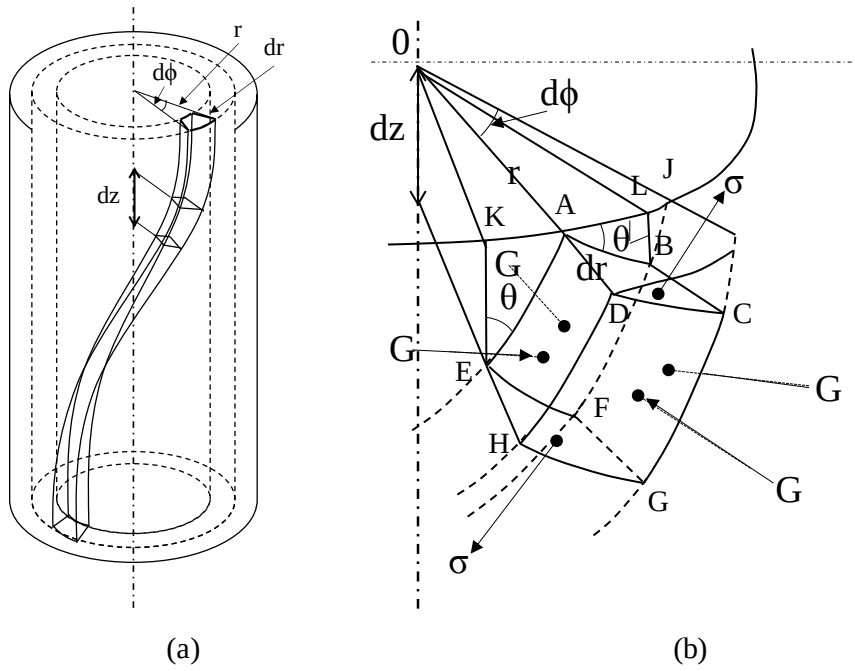

(a) (b)

Figure 2-8. Helically twisted yarn element (a) and expanded view of element (b)[31].

For radial equilibrium

$$\sigma\rho\sin^2\theta d\phi dr dz - G\rho\cos^2\theta d\phi dr dz + \rho\left(G + r\frac{dG}{dr}\right)d\phi dr dz = 0 \quad (21)$$

where ρ is fiber volume fraction(density). The first term is force acting across ABCD and EFGH(radial component of fiber tension) and second term is force acting on ADHE and BCGF(radial component of tangential transverse force) and third term is the difference between the forces on ABFE and DCGH(net radial force).

Equation 21 reduces to

$$rdG/dr = -(\sigma + G)\sin^2\theta$$
$$\frac{1}{r}\frac{dG}{dr} = -(\sigma + G)\frac{4\pi^2}{l^2} \quad (22)$$

Differentiating equation 14 with h constant,

$$2ldl = 8\pi^2 rdr \quad (23)$$

and substituting from equation 17

$$rdr = \frac{1}{4\pi^2}L^2 udu \quad (24)$$

Combining equation 20, 22 and 24

$$\frac{dG}{du} = -E_f \varepsilon_f \frac{1}{u}\left[\frac{c^2}{u^2} - \nu_{LT(yarn)}\left(1 - \frac{c^2}{u^2}\right) - (2\nu_{LT} - 1)G\right] \quad (25)$$

This a first-order differential equation is solved with the boundary condition that the transverse force is zero at the surface of the yarn(G=0 at u=1). Then compressive transverse stress is

$$G = E_f \varepsilon_y [\frac{1+\nu_{LT(yarn)}}{(1+2\nu_{LT})}\frac{c^2}{u^2}(1-u^{1+2\nu_{LT}}) - \nu_{LT(yarn)}\frac{1-u^{2\nu_{LT}-1}}{(2\nu_{LT}-1)}] \quad (26)$$

Now, it is considered that forces are developed on a yarn element. In case of short fiber yarns, slippage occurs near the end of yarns. Thus, a yarn element in this region is only considered(see Figure 2-9).

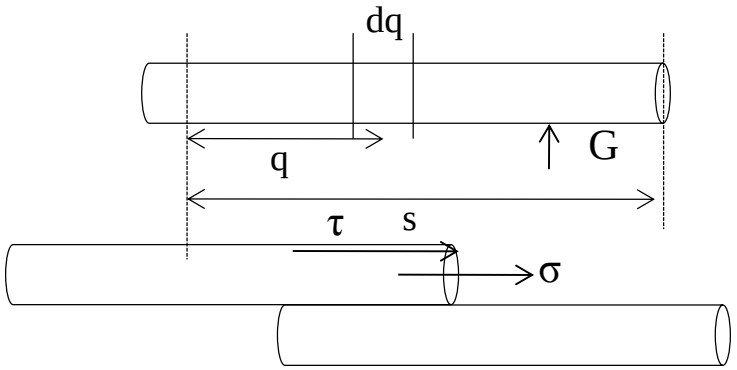

Figure 2-9. Development of forces on a yarn element[31].

When a fiber is pulled by dq, frictional force acts in the opposite direction. Then, the proportion of slippage length with respect to the fiber length is $(s-q)/L_f$, when the length of the fiber end is set to *s*. Since the force are contributing in the opposite direction, their effect is doubled and the frictional force is reduced by $1-2(s-q)/L_f$. Then maximum frictional stress is determined as

$$\tau = (\mu 2\pi a/\pi a^2)\int_0^s G(1-2(s-q)/L_f)dq \qquad (27)$$

where a is fiber diameter and μ is the frictional coefficient between individual CNTs. Then total axial stress on a fiber is

$$\sigma_{axial} = \int_0^s \tau ds + \frac{(L_f - s)}{L_f}\sigma \qquad (28)$$

Meanwhile, considering an annulus which thickness is *dr* in cross section of

the yarn, the axial stress(σ_{axial}) and the tangential stress *G* contribute to the yarn tension as Figure 2-10.

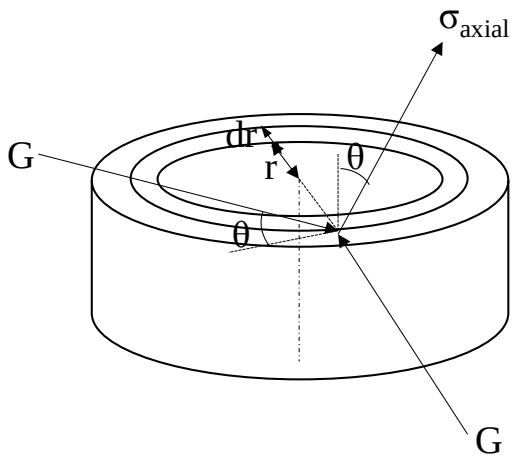

Figure 2-10. Direction of forces acting on yarn element[31].

Thus, yarn strength is

$$\sigma_{yarn} = \frac{2}{(1-c^2)} \int_c^1 \left[\sigma_{axial} \frac{c^2}{u^2} - G\left(1 - \frac{c^2}{u^2}\right) \right] u du \qquad (29)$$

2.3.2 Prediction of the tensile strength of CNT yarns

For calculating yarn strength(equation 29), numerous parameters should be determined. Young's modulus(E_f) of CNTs, axial Poisson's ratio(ν_{LT}) of CNTs, CNT diameter(a) and frictional coefficient(μ) between individual

CNTs were set as 1.13TPa, 0.048, 10nm and 0.9 which are same with values developed in statistical prediction approach(in chapter 2.2.3). Poisson's ratio of CNT yarns($\nu_{LT(yarn)}$) was established as 0.99 citing the result of Miao et al.[37]. From the results of tensile test(Figure 2-6), yarn strain(ε_y) was measured as 0.0564. In addition, fiber length(L_f) was measured as 150μm. Finally, two parameters(*u* and *s*) which have to be determined remain. *u* is radial position which varies from $c(\cos\alpha)$ at the center of the yarn to 1 at the surface and represents the radial position where failure occurs. *s* is the length near the end of individual CNTs where inter-CNT slippage occurs. These two values is not easy to be determined experimentally, thus used as variables, respectively. Then the strength of CNT yarns was predicted as Figure 2-11.

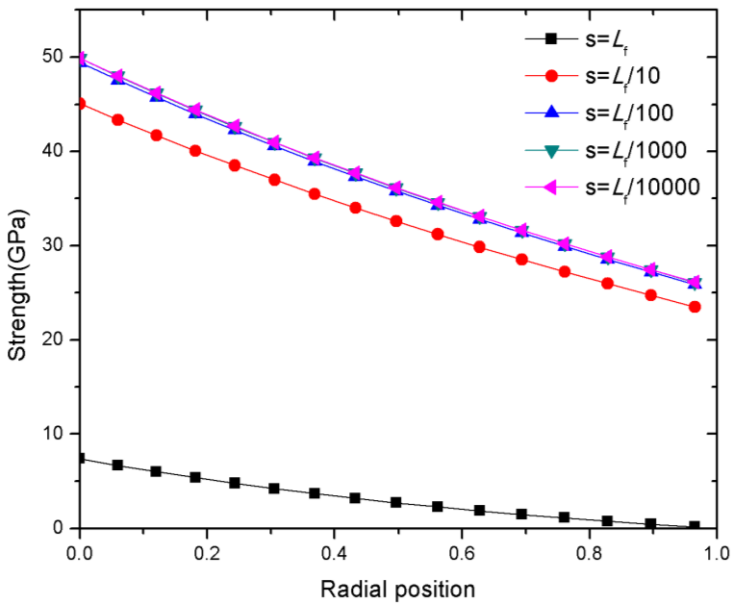

Figure 2-11. Predicted strength of CNT yarns according to the radial position.

Radial position varies from 0 at the center of the yarn to 1 at the surface and is represented as

$$\text{radial position} = \frac{r}{R} = \sqrt{\frac{u^2 - c^2}{1 - c^2}} \tag{30}$$

From the result, it was found that predicted strength decreases as radial position is closed to the surface of the yarn. At the center region, orientation angle of fibers is small with respect to the yarn axis and stronger lateral pressure is applied, thus the more stress are needed to break yarn. When *s*, the length of the fiber end where slippage occurs, is equal to fiber length(L_f), the yarn is broken by only frictional stress between individual fibers(see

black line in Figure 2-11). In this case, the prediction for yarn strength is between 140.73MPa(at the surface of the yarn) and 7.39GPa(at the yarn center). As *s* decreases, the effect of slippage decreases, thus the strength of short fiber yarns gets close to that of continuous filament yarns. Introducing parameters adopted in CNT yarn, when slippage length is 100 times less than fiber length, predicted strength is converged to the value between 26.12GPa(at the surface of the yarn) to 49.91GPa(at the yarn center). Comparing with experimental result(Figure 2-6), predicted value is still greater than the actual measurement, excepting the case that slippage length is equal to the fiber length and failure occurs near the surface. Indeed, packing density near the center is much higher than near the surface and most of CNTs exist in agglomerate form. Thus, the theoretical model based on mechanical approach cannot be applied to this portion. it was concluded that yarn fracture occurs at the region which radial position is higher than 0.5 and the major failure mechanism is highly depended on the inter-CNT slippage, since measured strength value is hundreds MPa order.

2.4 Conclusions

In this chapter, strength of CNT yarns was predicted from two previous yarn theories. At first, the statistical strength of CNT yarn was investigated using staple yarn theory developed by Pan. For the calculation, some parameters such as Young's modulus of CNT, frictional coefficient between CNTs and Weibull parameters representing stochastic strength of CNTs were cited from several literatures. In addition, structural mechanics considering the potential function in molecular dynamics(MD) to develop the effect of

inter-CNT friction. According to the short fiber theory, individual CNTs have to carry external force equally, however the existence of CNT agglomerate depending on the radial position, crimped and misaligned CNTs disturbed accurate prediction. Thus, the predicted value is much higher than experimental values, i.e. the actual measurement is two orders of magnitude lower than we predicted. Next, strength of CNT yarns was predicted from the theory of the mechanics of staple fiber yarns introduced by Hearle. For a given external force, the response of a yarn element such as the resultant deformation, the internal stresses and strains was calculated. Considering occurrences of inter-CNT slippage, yarn strength was predicted similar to the experimental values as long as slippage length is equal to the length of CNT. Thus, it was concluded that the major failure mechanism is highly depended on the inter-CNT slippage.

.

Chapter 3. Analysis of the mechanical behavior of CNT yarns using in-situ Raman spectroscopy

3.1 Introduction

Carbon nanotubes(CNTs) have been processed to yarns to utilize their excellent material properties such as high electrical conductivity, thermal conductivity and mechanical properties in micro/macro scale[12]. CNT yarns are appreciated as a useful structure with many promising applications in various field. In respect of the mechanical reinforcement, it is not easy to disperse CNTs in the matrix material so that it results in low aspect ratio of the reinforcement. However, by Using CNT yarns, high-volume fraction reinforcement composites with excellent mechanical properties can be manufactured[44]. In addition, CNT yarns are high strength/toughness fibers as well as conducting material, it has applications in flexible electronic devices such as flexible supercapacitor, electrodes, fiber solar cell etc., using yarn itself and arranging yarns[45-47]. Furthermore, they can react mechanically with electric source. CNT yarns can be utilized as sensors or actuators[48, 49].

CNTs have highly anisotropic electrical, optical, mechanical, and thermal properties, i.e. the physical properties of CNT is best in the axial direction. Thus, it was important to arrange CNTs in a particular direction in CNT/Polymer composites and CNT assemblies field[50, 51]. In the same vein, for good understanding of the properties of CNT yarns, the orientation

of individual CNTs in the yarn should be accurately determined. Inner structure of CNT yarns can be understood approximately according to the classical yarn theory[52]. Orientation angle of fibers in the yarn with respect to the axial direction decreases from surface to the center with existence of fiber migration, i.e. some fibers which are on the surface at one point along the yarn must be inside the yarn at other points. However, due to the existence of Van der Waals interactions between individual CNTs, CNT yarns have a little different inner structure comparing to the yarn structure based on the classical yarn theory. Sears et al.[43] investigated the internal structure of CNT yarns was revealed using focused ion beam milling. It was investigated that CNT yarns have core-sheath structure, i.e. CNTs in the core region are highly packed so that they are bundled due to Van der Waals interactions while CNTs near the sheath exist less bundled. The inner structure would be deformed complicatedly when CNT yarns receive external forces. Therefore, the inner structure of CNT yarns should be characterized as they changed according to applied external force.

Raman spectroscopy, which is an inelastic photon scattering spectrum, has been widely used as a non-destructive method to investigate the structure such as the diameter and chirality related to their metallic or semiconducting properties[53-56]. In addition, using polarized spectra, the intensity of the G band in the Raman spectra depends on the orientation of CNT, i.e. as orientation angle of the nanotube axis with respect to the direction of the polarizer increases, the intensity decreases monotonously[51, 57, 58]. There are two types of measurement in Polarized Raman spectroscopy, VV and VH measurement. For VV measurement, the direction of polarizer is parallel

with the analyzer which catches scattered light and the intensity is proportional to $\cos^4\theta$ where θ is the angle between the CNT axis and polarization direction. For VH measurement, the direction of polarizer is perpendicular to the analyzer and the intensity is proportional to $\cos^2\theta\sin^2\theta$ [58]. Therefore, polarized Raman spectroscopy has been commonly utilized to investigate orientation of CNT based composites and assemblies[59]. Meanwhile, the shift of the Raman bands greatly depends on the deformation modes, since the variation of bond length or force constant of C=C induce different electronic properties and phonon vibration. Thus, it will shift upwards under a uniaxial compression, and shift downwards under tension[60]. Therefore, deformation of CNTs under external force can be measured using *in-situ* Raman spectroscopy. Deformation of CNT fibers(yarns), films and CNT/Polymer composites were studied using knowledge of peak shift[61, 62]. Indeed, Raman band shift provides several information related to the deformation such as stress concentration and elastic modulus of CNTs and its composites[59, 63, 64]. As stated above, in the previous research, the orientation distribution and deformation of CNT yarns were studied using Raman spectroscopy, however no attempts have been made to analyze the orientation of CNTs in the yarn at concurrence. The task of obtaining quantitative descriptions of structural changes during deformation should be needed to allow sufficient comprehension of the mechanisms responsible for the deformation characteristics.

In this chapter, the mechanical behavior of CNT yarns, which were manufactured by twisting CNT sheets drawn from CNT forest, was investigated by using *in-situ* Raman spectroscopy. An in-situ micro Raman

spectroscopy system used for investigating the mechanical behavior of the CNT yarn under external force(see Figure 3-1). The effect of the tension and torsion on the CNT orientation within CNT yarns was quantitatively characterized using the fiber orientation function, which was determined by the intensity of the G band in the Raman spectra of CNT yarns. The shift of Raman band was also observed to investigate the mechanical deformation of individual CNTs within CNT yarns.

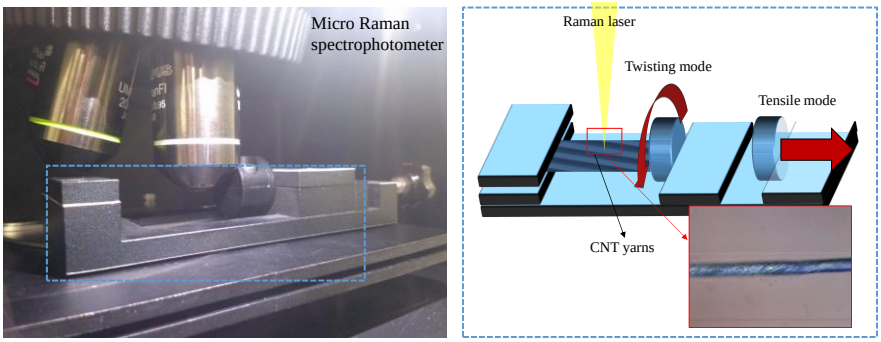

(a) (b)

Figure 3-1. An *in-situ* micro Raman spectroscopy system used for investigating the mechanical behavior of the CNT yarn under external force. (a) Tensile and torsional loading device. (b) A schematic diagram illustrating obtainment Raman spectra during *in-situ* tensile and torsion test.

3.2 Characterization

3.2.1 Penetration depth

According to Beer-Lambert law, the intensity of a Raman laser penetrating a CNT yarn falls off for the relationship, $I = I_0 e^{-\alpha z}$, where I_0 is the intensity of the incident light, α is the absorption coefficient which is depended on the material and z is thickness of the material. Penetration depth is defined as $1/\alpha$ which the intensity decays to $1/e$ of its surface value. Therefore, the penetration depth should be known to identify the measured area of the CNT yarns. Because CNT yarns were manufactured by twisting CNT sheets, CNT sheets were laid on a silicon wafer and then the intensity decrease of the silicon peak was measured according to the thickness of CNT sheets. The averaged thickness of CNT sheets were measured using atomic force microscopy(AFM, Park system XE100) with non-contact mode. Scan size and scan rate were set as 10μm X 10μm and 1Hz, respectively.

3.2.2 Orientation distribution function(ODF)

The orientation of individual CNTs was described by Euler angles (θ,φ,ε), which are a means of represent the spatial orientation of a frame of CNT yarn as a composition of rotations from a frame of individual CNTs(see Figure 3-2). θ is the polar angle between axes of CNT and CNT yarn. φ is the azimuthal angle between x axis and the intersection of the xy and the XY coordinate planes(N-axis). ε is the azimuthal angle between X axis and N-

axis.

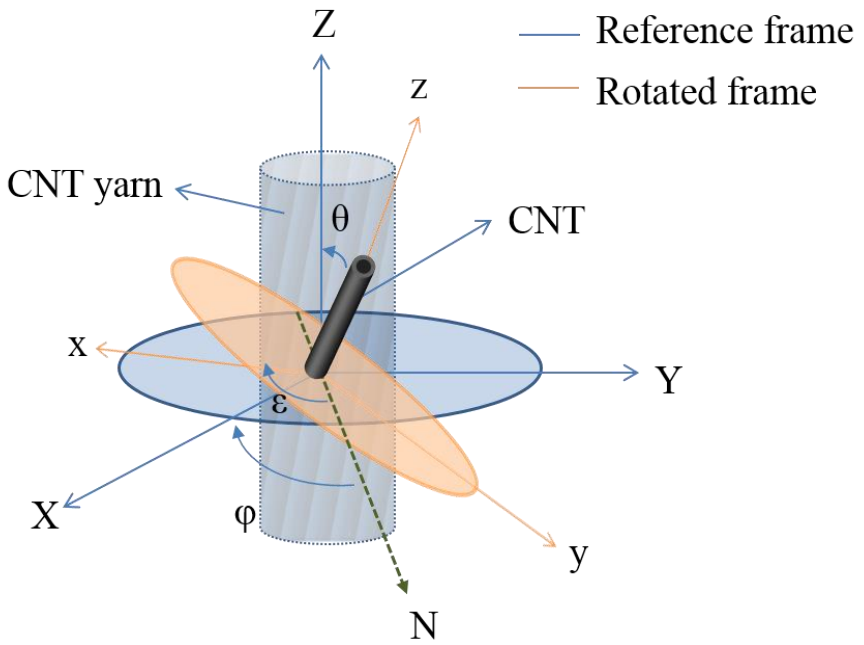

Figure 3-2. Euler angles to represent the orientation angle of individual CNT inside CNT yarn.

Orientation distribution function(ODF), $f(\theta,\varphi,\varepsilon)$, is a probability density function and $f(\theta,\varphi,\varepsilon)\sin\theta d\theta d\varphi d\varepsilon$ is the probability of finding an individual CNT in CNT yarn between (θ,φ,ε) and (θ +dθ,φ +d φ,ε +dε). Since CNT possess the cylindrical symmetry, angle ε does not involve the ODF expression and for an axially symmetric structure like a yarn it is easy

to see that the azimuthal angle φ is uniformly distributed. In other words, angle φ also is not included in ODF, so that ODF is only function of θ, $f(\theta)$, which is the angle between axis of nanotube and axis of yarn[57]. Then, the ODF is given by the maximum entropy formalism[65, 66] as followings:

$$f(\theta) = A\exp[-(\lambda_2 P_2(\cos\theta) + \lambda_4 P_4(\cos\theta))] \qquad (1)$$

where $P_i(\cos\theta)$ is the Legendre polynomials of degree i and coefficients A, λ_2 and λ_4 should be determined to complete ODF as followings:

$$\begin{aligned}
&\int_0^{2\pi}\int_0^{2\pi}\int_0^{\pi} f(\theta)\sin\theta d\theta d\varphi d\varepsilon = 1 \\
&\int_0^{2\pi}\int_0^{2\pi}\int_0^{\pi} P_2(\cos\theta) f(\theta)\sin\theta d\theta d\varphi d\varepsilon = < P_2(\cos\theta) > \qquad (2) \\
&\int_0^{2\pi}\int_0^{2\pi}\int_0^{\pi} P_4(\cos\theta) f(\theta)\sin\theta d\theta d\varphi d\varepsilon = < P_4(\cos\theta) >
\end{aligned}$$

where $< P_i(\cos\theta) >$ is the average value of the Legendre polynomials of degree i and determined by the polarized Raman scattering intensity of CNT yarns solving the following equations[57]:

$$\begin{aligned}
&\frac{I^{VV}{}_{CNTyarn}(\Phi=0)}{I^{VH}{}_{CNTyarn}(\Phi=0)} = \frac{I^{VV}{}_{CNTyarn}(\Phi=0)}{I^{VH}{}_{CNTyarn}(\Phi=90)} = -\frac{24 < P_4(\cos\theta) > +60 < P_2(\cos\theta) > +21}{12 < P_4(\cos\theta) > -5 < P_2(\cos\theta) > -7} \qquad (3) \\
&\frac{I^{VV}{}_{CNTyarn}(\Phi=90)}{I^{VH}{}_{CNTyarn}(\Phi=0)} = \frac{I^{VV}{}_{CNTyarn}(\Phi=90)}{I^{VH}{}_{CNTyarn}(\Phi=90)} = \frac{-9 < P_4(\cos\theta) > +30 < P_2(\cos\theta) > -21}{12 < P_4(\cos\theta) > -5 < P_2(\cos\theta) > -7}
\end{aligned}$$

Using tangential shear mode(G), the G band at 1500~1605cm^{-1}, the intensity was measured by employing polarized Raman spectroscopy. According to

the angle between direction of polarizer and the analyzer that catches scattered light, there are two modes, VV mode and VH mode. When the polarization direction of both polarizer and analyzer are parallel with each other, I_{VV} is measured. When the polarization direction of polarizer are perpendicular to the analyzer, I_{VH} is measured. Φ is the angle that axis of CNT yarn arranges with respect to the direction of polarizer.

3.2.3 Peak shift

The shift of the Raman bands greatly depends on the deformation modes (compressive and tensile modes). Bands shift upwards or downward under uniaxial compressions or tension. The tensile behavior and torsional behavior of CNT yarns were studied by investigating the deformation of individual CNTs, which can be characterized by the peak shift.

3.3 Experimental

The polarized Raman scattering spectra of CNT yarns were recorded with a JASCO NRS-3100 micro Raman spectrophotometer(1800 lines/mm grating and high sensitivity cooled CCD). Raman spectra were acquired at 532 nm excitation and microscope objective 100x was used. The focused laser spot size was 2μm with a laser power of 2.6mW. The Raman data were collected over the 1000-2000 cm^{-1} range at a resolution of 1.87 cm^{-1}.

3.4 Results and discussion

In-situ tensile and torsional test were performed under polarized Raman

spectroscopy. The penetration depth of Raman laser into CNT yarns was measured as 465.11nm with the standard deviation of 194.17nm. The internal structure is different depending on the radial position, i,e. individual CNTs are highly packed in the core and packing density become lower from the core to the sheath. Thus, observations of the various parts in the yarn is required, since the mechanical behavior also depends on the radial position. In order to investigate various parts of the yarn, CNT yarns with different diameters were fabricated. To investigate tensile behavior, changes near the CNT yarn surface were observed using yarns with a diameter of about 10μm, while CNT yarns with the diameter of less than 1μm were used to measure the change of the whole yarn. In case of torsional behavior, it was assumed that the core part consisted of highly packed does not contribute to torsional mechanism. CNT yarns which diameter is about 10μm were fabricated.

For investigating tensile behavior, Raman spectra was obtained for CNT yarns with 1cm gauge length at various strain level. Figure 3-3 shows measured orientation distribution changes near the surface area at different strain level. At low strain, the orientation angle with respect to the tensile direction decreased slightly(see Figure 3-3(a) and (b)). As the CNT yarn was tensioned further, more CNTs were rotated to the tensile direction(see Figure 3-3(c) and (d)).

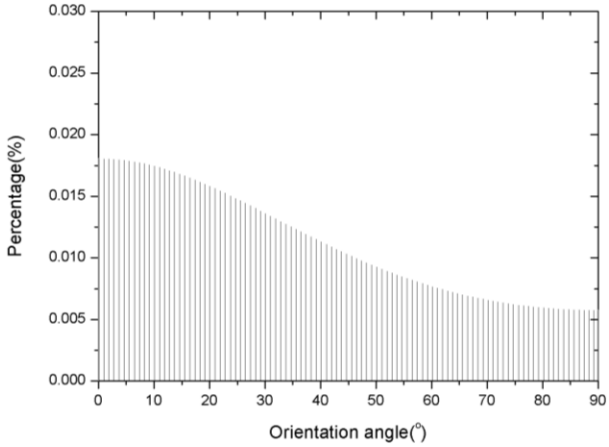
0.030
0.025
0.020
0.015
0.010
0.005
0.000
Percentage(%)
0
10
20
30
40
50
60
70
80
90
Orientation angle(°)

(a)

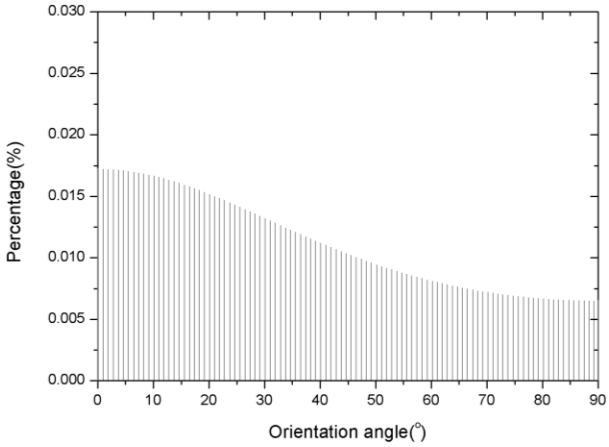
0.030
0.025
0.020
0.015
0.010
0.005
0.000
Percentage(%)
0
10
20
30
40
50
60
70
80
90
Orientation angle(°)

(b)

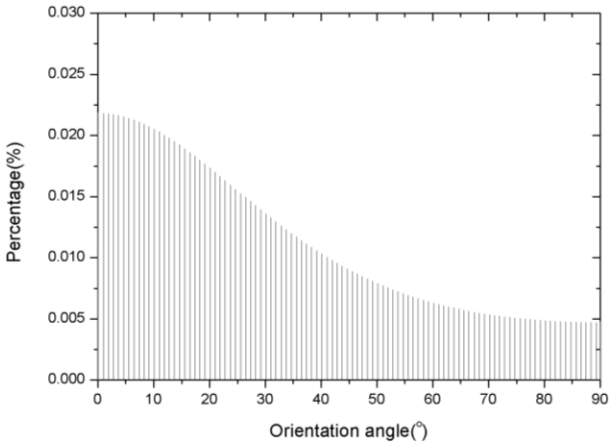

(c)

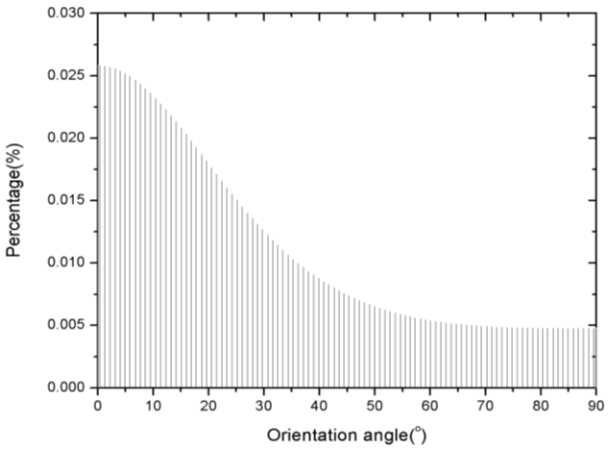

(d)

Figure 3-3. Distribution of the CNT orientation angles in CNT yarn (diameter:10μm) according to strain level. (a) 0, (b) 0.009, (c) 0.0378, and (d) 0.063.

According to the classical yarn mechanics, the orientation angle decreases when the yarn receive tension considering the idealized helical yarn structure, i.e. orientation angle with respect to the axial direction decreases from surface to the center. Despite of consideration of fiber migration, i.e. fibers which are on the surface at one point along the yarn must be inside the yarn at other points, it is uncertain that orientation angle does not change depending on the tension. To investigate this phenomenon in CNT yarns, angle changes among strain levels were calculated. At low strain(from 0 to 0.009), individual CNTs rotated 2.40° according to the direction perpendicular to tensile direction. When strain changes from 0.009 to 0.0378 and from 0.0378 to 0.063, angle changes to 7.18° and 3.04° with respect to the tensile direction, respectively. Unusual angle changes at low strain have similarities with a mechanism of migration[52](Figure 3-4).

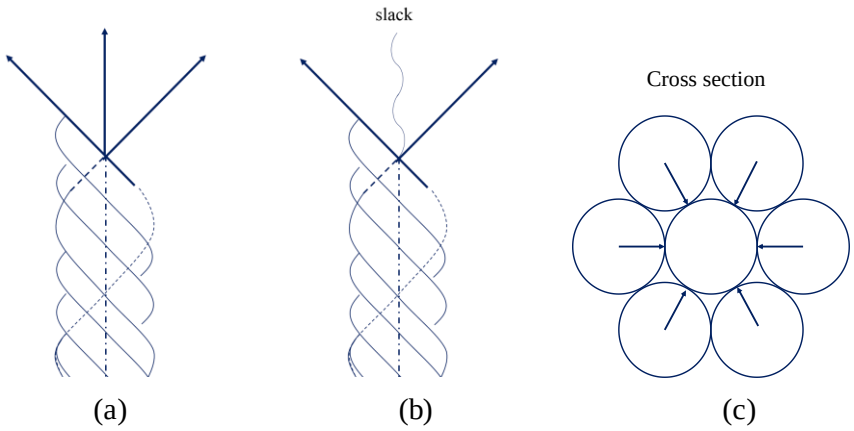

Figure 3-4. A mechanism of migration. (a) Central fiber under tension. (b) Central fiber slack allowing migration. (c) Pressure from surrounding fibers.

According to the mechanism, extremely difficult case to change position of fibers is considered, i.e., hexagonal closed packed yarn is consisted of 7 fibers. Among that fibers, central fiber is not easy to move when every fibers receive tension(Figure 3-4(a)). Therefore, some conditions are necessary to push the fiber out from a central position as followings. Central fiber becomes slack and buckles(Figure 3-4(b)). Then, the fiber should overcome the pressure from surrounding fibers(Figure 3-4(c)). In other words, when individual CNT does not receive tension properly, CNT changes their position rather than rotate to the tensile direction. Meanwhile, overall angle change under tension with respect to the initial angle was compared to the theoretical calculation(Figure 3-5)[52].

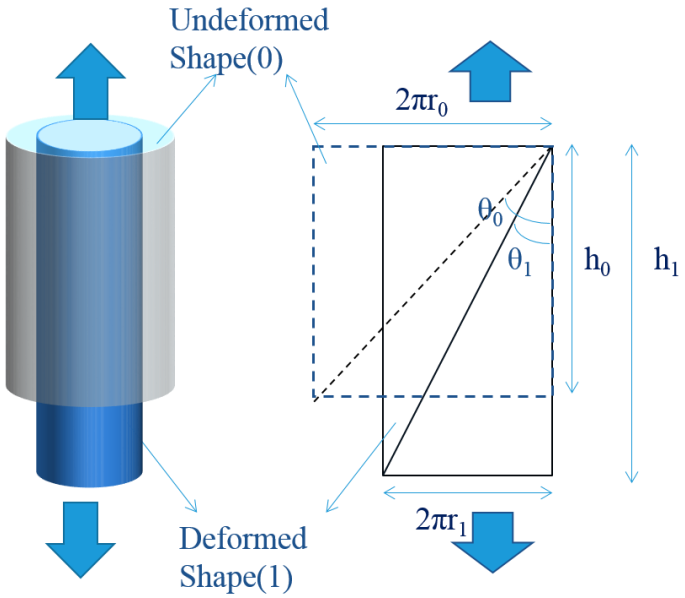

Figure 3-5. Geometry of yarn under tensile strain[52].

Surface angle before and after applying strain was theoretically calculated regarding the yarn as cylinder as following equation:

$$\tan\theta_1 = \frac{\tan\theta_0}{(1+\varepsilon_y)^{3/2}}\sqrt{\frac{V_1}{V_0}} \qquad (4)$$

where θ, V and ε_y are the surface angle, yarn volume and yarn strain, respectively. Notation 0 and 1 mean undeformed and deformed state. θ_0, $\frac{V_1}{V_0}$ and ε_y were experimentally measured as 19°, 0.75 and 0.063,

respectively. In this case, orientation change was calculated as 4.72° and the value is lower than experimental value, i.e. much more CNTs were rotated and it is estimated that CNTs does not rotate individually and bundled CNTs rotate. The peak shift which shows deformation of constituent CNTs was investigate to tensile behavior near the surface region in addition to orientation distribution changes(see Figure 3-6).

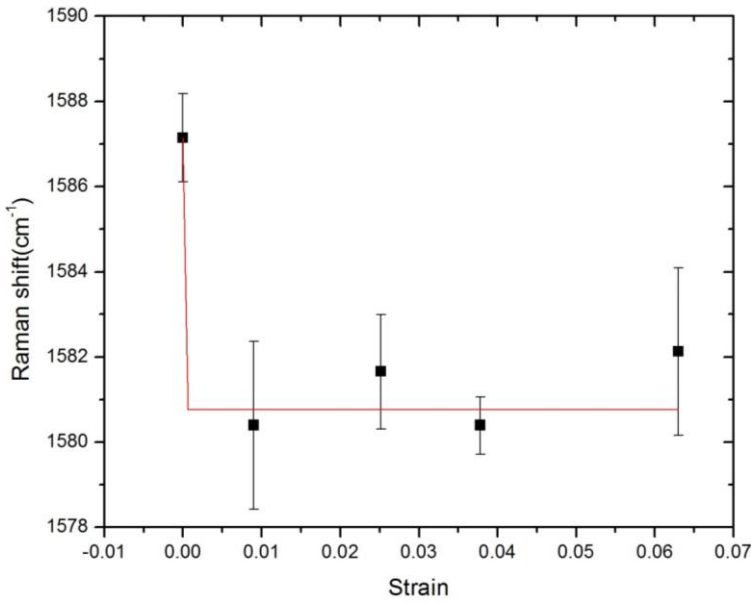

Figure 3-6. Raman band shift of CNT yarn (diameter:10μm) according to strain level.

At low strain level, Raman band shifts largely. As the strain is applied to yarn more and more, a dramatic shift in Raman band does not appear any

longer, meaning that several CNTs move and rotate rather than they are stretched. Although yarn strain increases, rotation of CNTs is limited. It means that inter-bundle slippage occurs without carrying external forces. Summarizing tensile behavior near the yarn surface, when CNT yarns receive tension initially, individual CNTs receive tension irregularly. Then they are reoriented to fill the empty space in the yarn and some of them are bundled. As strain increases, the number of CNT bundle increases and CNT bundles are rotated and inter-bundle slippage occurs without receiving tension. Expanding investigation region of the yarn, the same experiment using CNT yarns with the diameter of less than 1μm was carried out to measure the change of the whole yarn. Note that the penetration depth we measured was about 500nm. Figure 3-7 shows measured orientation distribution changes of the whole yarn at different strain level. In comparison to the changes near the surface, the orientation angle changed drastically at low strain(see Figure 3-7(a) and (b)). As the CNT yarn was strained from 0.008 to 0.0333, CNTs were rotated to the tensile direction. Meanwhile, there were few changes in orientation distribution when strain increases to 0.046.

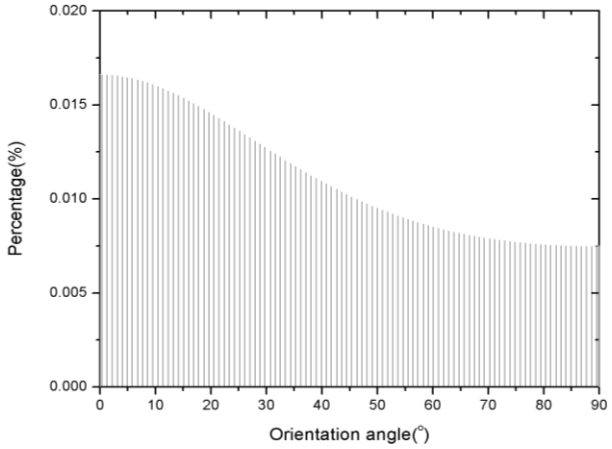
0.020
0.015
0.010
0.005
0.000
Percentage(%)
0
10
20
30
40
50
60
70
80
90
Orientation angle(°)

(a)

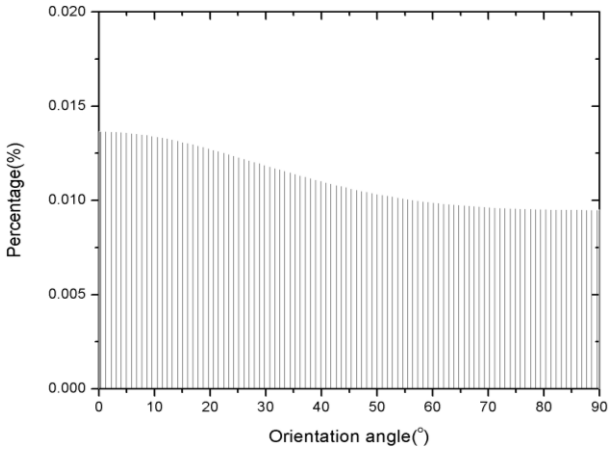
0.020
0.015
0.010
0.005
0.000
Percentage(%)
0
10
20
30
40
50
60
70
80
90
Orientation angle(°)

(b)

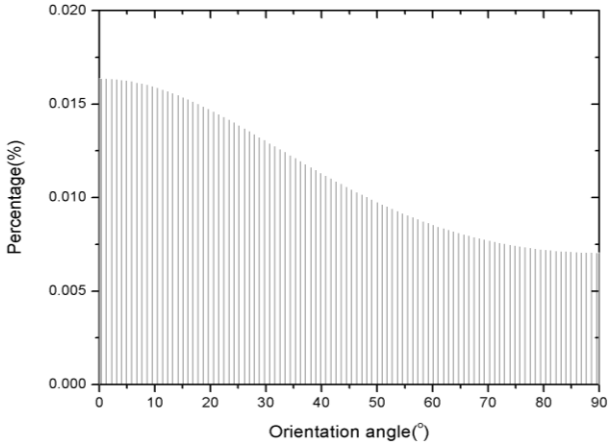

(c)

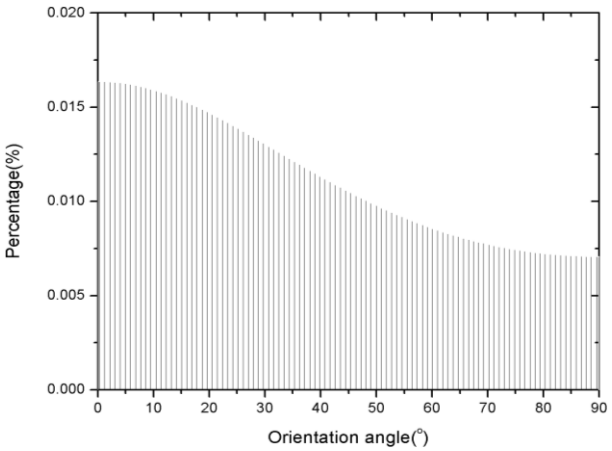

(d)

Figure 3-7. Distribution of the CNT orientation angles in CNT yarn (diameter:1μm) according to strain level. (a) 0, (b) 0.008, (c) 0.0333, and (d) 0.046.

It was estimated that inter-bundle slippage occurs, since angle change is very small despite of existence of yarn strain. Note that changes of the whole yarns also include changes near the surface region. Thus, the increment in orientation angle reflects that more CNTs were reoriented to change their radial position and to fill the empty space in the yarn. Meanwhile, overall, there were few changes in orientation angle as strain increases from 0 to 0.046, since CNTs near the center of yarn were not easy to move or rotate due to the lateral pressure, so that the orientation angle change was small. The effect of the lateral pressure also appears in Raman band shift (see Figure 3-8).

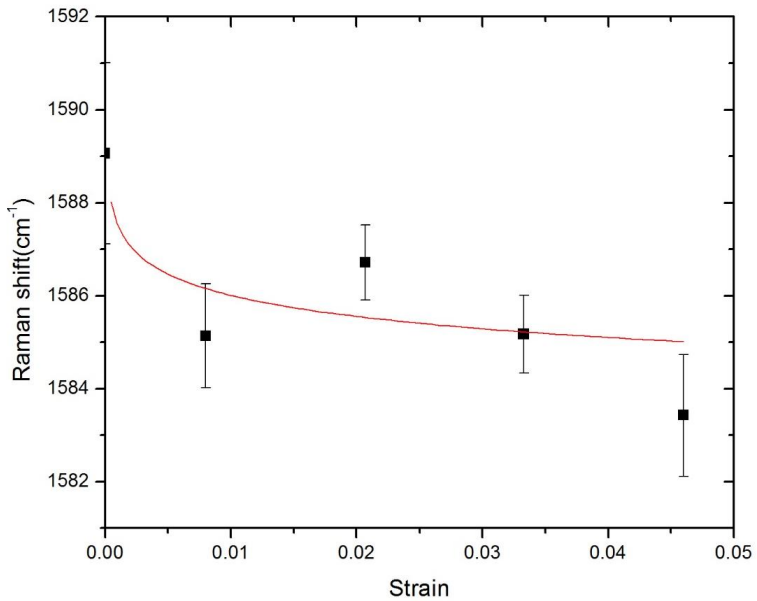

Figure 3-8. Raman band shift of CNT yarn (diameter:1μm) according to strain level.

The amount of shift is less than 10 μm diameter yarn case, but the peak shift downwards continuously. This represents that CNTs were slightly stretched as the strain increased. CNTs in the center region are highly packed so that they are already bundled before receive tension. Therefore, bundled CNTs near the center region could receive tension due to the existence of the lateral pressure by surrounding helically wound CNTs. Some CNTs in bundle could get tension continuously, but every CNTs in the bundle could not. It is estimated that CNTs which receive tension exist partially in CNT bundles near the center region. Furthermore, CNTs near the surface region could carry external forces only at low strain, thus this phenomenon still appears as high decrease comparing to the decrement at other strain levels. While strain increases from 0.008 to 0.0207, few increment of band shift reflect that CNTs near the surface region does not carry external forces anymore, instead CNTs in the yarn receive compression. As long as CNT bundles near the center are surrounded by other bundles of CNTs, some CNTs in the bundle can receive tension due to the effect of lateral pressure as strain increases more.

Summarizing the results, the tensile behavior of CNT yarns can be explained as follows: individual CNTs are stretched at low strain, while CNTs move to fill in empty space. They are partially compacted by Van der Waals interaction while CNTs are reoriented to the tensile direction. Compacted CNTs are combined with each other, forming CNT bundles, followed by the rotation of bundles to the tensile direction. Finally, bundle slippage and break occur at the interfaces between CNT bundles.

For investigating torsional behavior, experiment was setup as Figure 3-9. Torsional mechanisms are different according to the boundary conditions, i.e.

one-end tethered yarns can rotate much higher than two-end tethered yarns, but the operation is irreversible[49]. Experiment was conducted using CNT yarns which length is 5cm and CNT yarns were untwisted(-80turns/cm) first and then twisting(80turns/cm) was applied to the yarn. In case of one-end tethered yarns, the rotation is simply depended on the distance from the fixed region as $\phi(x) = x\Delta\theta$ [49]. Where ϕ is the rotation, x is the distance from the tethered end to rotated part and $\Delta\theta$ is the rotation per yarn length. Therefore, two parts in the yarn was investigated, i.e. one is near the fixed region and the other is near the region applying untwist and twist. Generally, orientation angle decreases when yarn is untwisted and increases when yarn is twisted.

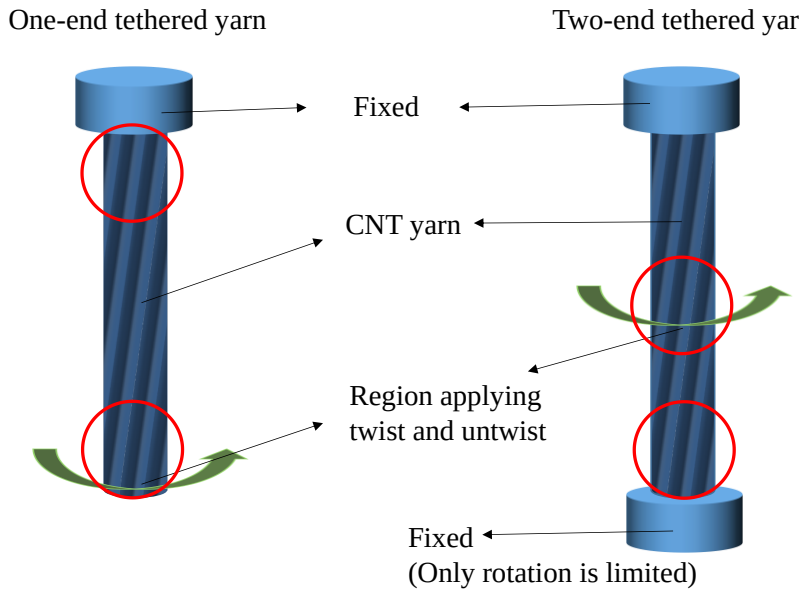

Figure 3-9. One-end tethered and two-end tethered yarn configuration for investigating torsional behavior of CNT yarns. Marked area with red line means measurement area to obtain Raman spectra.

Figure 3-10 shows orientation distribution changes near the paddle and general yarn deformation under torsion was presented. However, there was unusual changes near the fixed region(see Figure 3-11), i.e., very large amount of CNTs changes their orientation angle and orientation distribution does not return to the original state before the yarn receives torsion. To investigate the unusual changes, structural changes were observed by scanning electron microscope(SEM) in these conditions(see Figure 3-12).

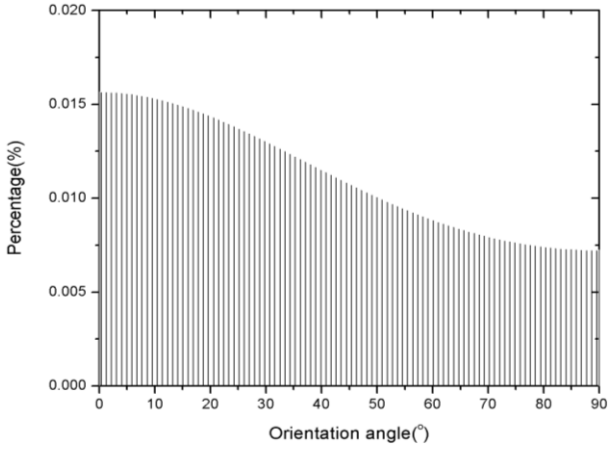
0.020
0.015
0.010
0.005
0.000
Percentage(%)
0
10
20
30
40
50
60
70
80
90
Orientation angle(°)

(a)

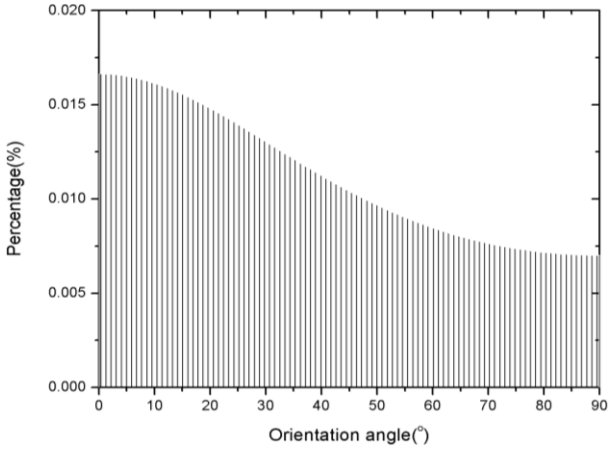
0.020
0.015
0.010
0.005
0.000
Percentage(%)
0
10
20
30
40
50
60
70
80
90
Orientation angle(°)

(b)

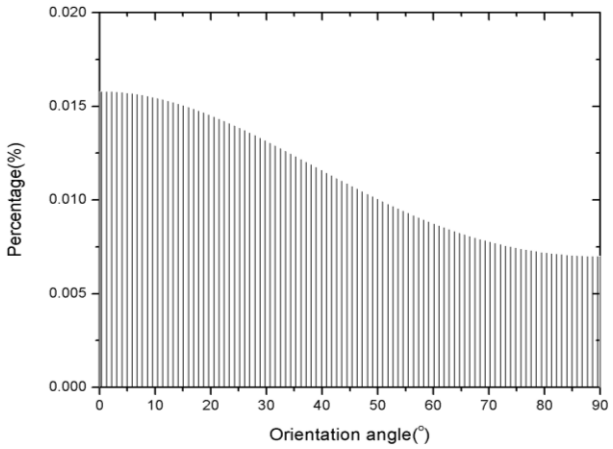

(c)

Figure 3-10. Distribution of the CNT orientation angles near the rotated part in one-end tethered CNT yarn according to the applied torsion. (a) Initial orientation angle distribution. (b) Orientation angle distribution after untwisting(-80turns/cm) process. (c) Orientation angle distribution after re-twisting(+80turns/cm) process.

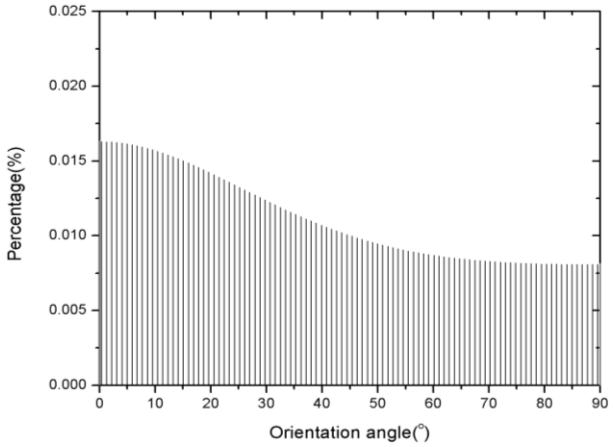
0.025
0.020
0.015
0.010
0.005
0.000
Percentage(%)
0
10
20
30
40
50
60
70
80
90
Orientation angle(°)

(a)

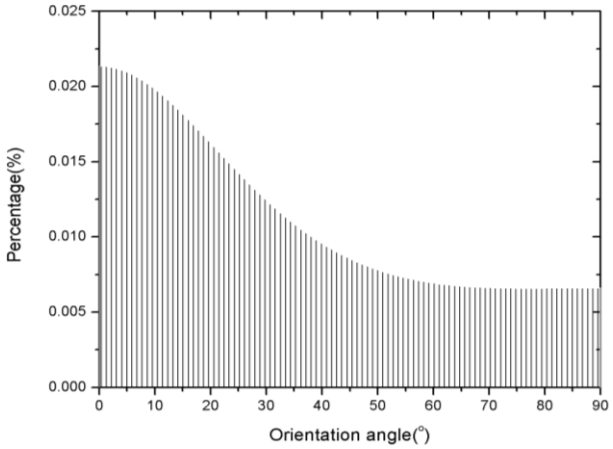
0.025
0.020
0.015
0.010
0.005
0.000
Percentage(%)
0
10
20
30
40
50
60
70
80
90
Orientation angle(°)

(b)

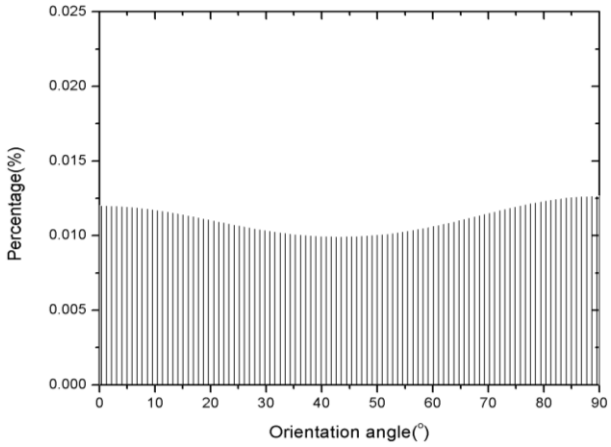

(c)

Figure 3-11. Distribution of the CNT orientation angles near the fixed region in one-end tethered CNT yarn according to the applied torsion. (a) Initial orientation angle distribution. (b) Orientation angle distribution after untwisting(-80turns/cm) process. (c) Orientation angle distribution after re-twisting(+80turns/cm) process.

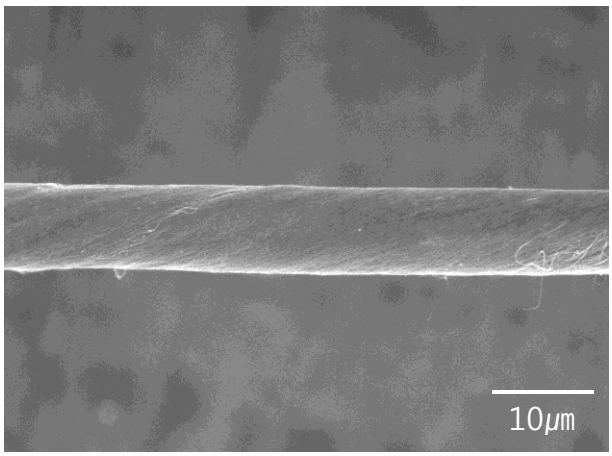

(a)

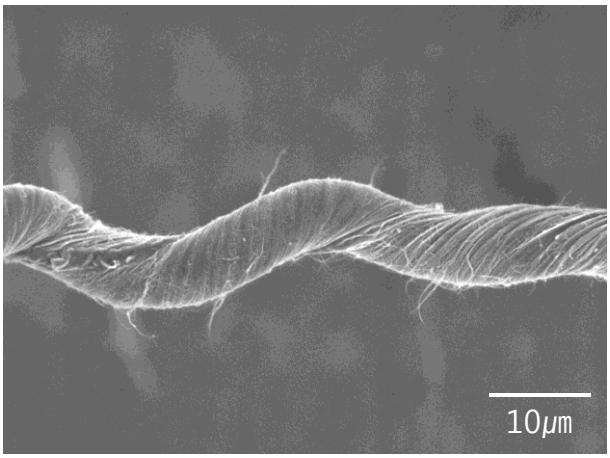

(b)

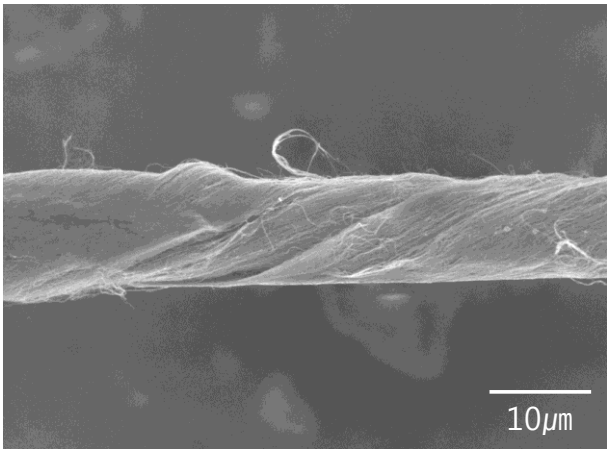

(c)

Figure 3-12. Structural changes near the fixed region in one-end tethered CNT yarn during untwisting and re-twisting process. (a) Initial state. (b) false twist appeared after untwisting(-80turns/cm) process. (c) Permanent deformed yarn shape after re-twisting(+80turns/cm) process.

It was found that false twist occurs during untwisting process and it does not return to the original shape. In other words, this part was deformed permanently during re-twisting. Generally, yarn twists and untwists on the basis of the yarn axis under external torsion. However, when the yarn is untwisted, strong elastic forces developed during twisting operation are relieved. Thus, yarn axis is coiled or takes away from the axis of rotation and these configuration was denominated as snarl(see Figure 3-13)[67]. When CNT yarns including numerous turns of CNTs are untwisted, the high torque forces developed were relieved by the formation of snarls, but snarls deformed yarn configuration permanently. As a results, one-end tethered

yarn rotates irreversibly due to the formation and disappearance of snarls. In case of two-end tethered yarn, two parts in the yarn was investigated, i.e. one is near the fixed region and the other is near the middle of yarn. Note that external torsion was applied to the middle of yarn.

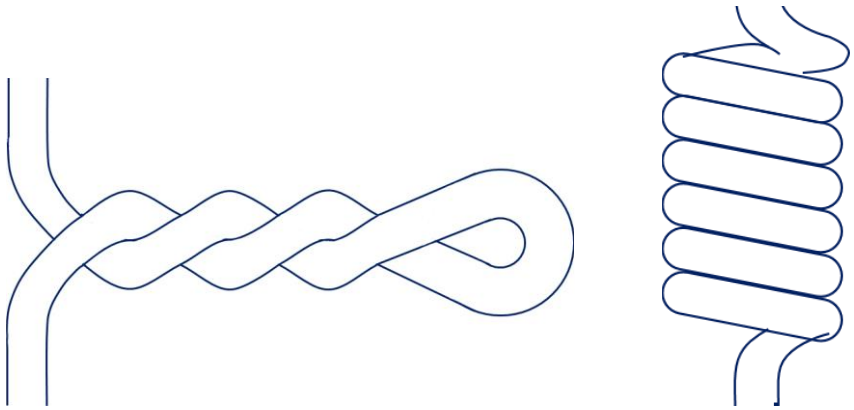

(a) (b)

Figure 3-13. Formation of snarls. (a) Normal snarl. (b) Cylindrical snarl.

Figure 3-14 shows orientation distribution changes near the fixed region and general yarn deformation under torsion was presented. However, near the middle of yarn, orientation angle decreases when yarn is untwisted and increases when yarn is twisted, i.e. CNTs in near the fixed region and middle part are rotated in opposite directions(see Figure 3-15).

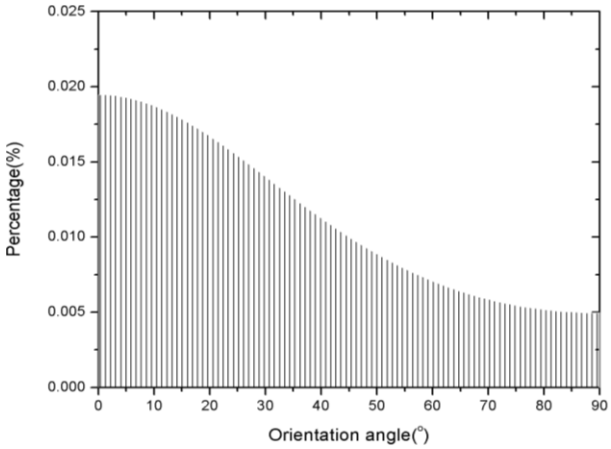
0.025
0.020
0.015
0.010
0.005
0.000
Percentage(%)
0
10
20
30
40
50
60
70
80
90
Orientation angle(°)

(a)

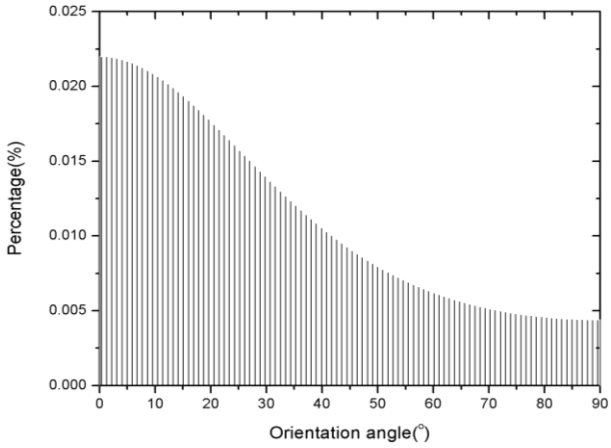
0.025
0.020
0.015
0.010
0.005
0.000
Percentage(%)
0
10
20
30
40
50
60
70
80
90
Orientation angle(°)

(b)

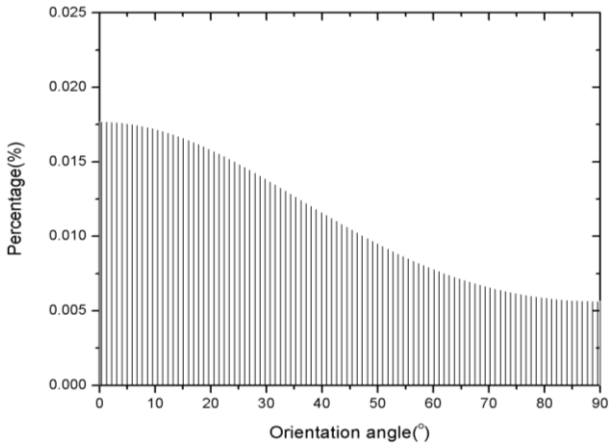

(c)

Figure 3-14. Distribution of the CNT orientation angles near the fixed region in two-end tethered CNT yarn according to the applied torsion. (a) Initial orientation angle distribution. (b) Orientation angle distribution after untwisting(-80turns/cm) process. (c) Orientation angle distribution after re-twisting(+80turns/cm) process.

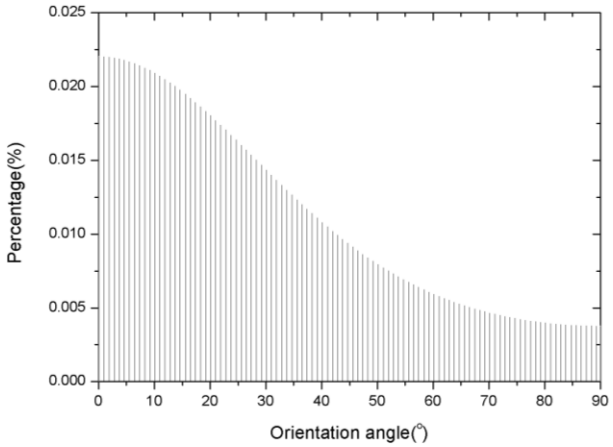
0.025
0.020
0.015
0.010
0.005
0.000
Percentage(%)
0
10
20
30
40
50
60
70
80
90
Orientation angle(°)

(a)

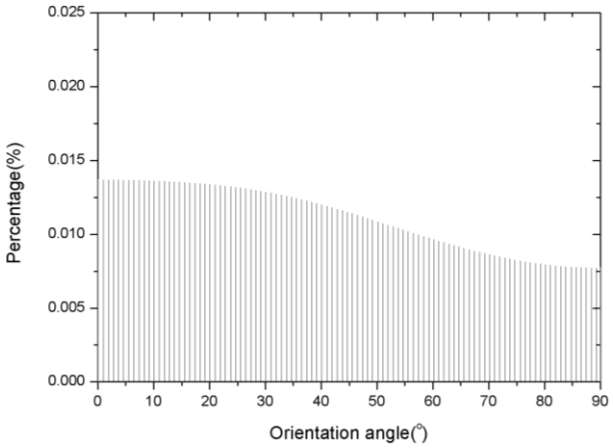
0.025
0.020
0.015
0.010
0.005
0.000
Percentage(%)
0
10
20
30
40
50
60
70
80
90
Orientation angle(°)

(b)

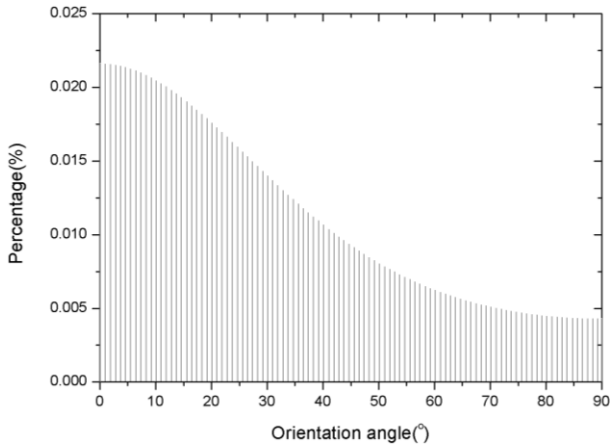

(c)

Figure 3-15. Distribution of the CNT orientation angles near the middle of two-end tethered CNT yarn according to the applied torsion. (a) Initial orientation angle distribution. (b) Orientation angle distribution after untwisting(-80turns/cm) process. (c) Orientation angle distribution after re-twisting(+80turns/cm) process.

Since rotation is restricted at both ends of the yarn, some parts should be twisted to maintain torque equilibrium, thus twisting occurs at concurrence when the yarn is untwisted. Meanwhile, there are three influences on torsion of yarns, which are bending moment and torsional moment of constituent CNTs in addition to torque due to yarn tension. However, in case of CNT yarns, Van der Waals forces among individual CNTs also have an effect on the torsional behavior. When more twist is inserted into the CNT yarn, the whole structure of the yarn grows tighter, i.e. individual CNTs get closer to

the equilibrium distance. Thus, twisting is more advantageous than untwisting so that orientation angle near the middle of the yarn changes larger comparing to angle changes near the fixed region(see Figure 3-14 and Figure 3-15). In the previous researches[49, 68], it was founded that yarn length decreases despite CNT yarns are untwisted in case of two-end tethered yarn. Note that if the effect of boundary conditions is absent, yarn length increases during untwisting and decreases during twisting. The effect of differences in the amount of angle changes leads to the yarn contraction while additional moments are generated by yarn contraction to maintain torque equilibrium. In conclusion, when CNT yarns are untwisted, the high torque forces are relieved by twisting in opposite way without the formation of snarls maintaining torque equilibrium so that two-end tethered yarn rotates reversibly.

3.5 Conclusions

The mechanical behavior of CNT yarns was investigated using *in-situ* polarized Raman spectroscopy. For investigating tensile behavior, changes in the ODF and Raman band shift were examined at different strain levels using different diameter yarns. It was concluded that CNTs in the center receive tension continuously, but CNTs in the surface get tension only at low strain. CNT bundles, which are highly compacted CNTs caused by Van der Waals interaction, were created when CNT yarn is tensioned. The torsional behavior of CNT yarns was investigated according to the boundary conditions, which are one-end tethered and two-end tethered conditions. Changes in the ODF and Raman band shift were examined during untwisting and re-twisting process. It was found that in case of one-end tethered yarns, false twist and permanent deformation occur, results in irreversible torsional

behavior. In case of two-end tethered yarns, high torque forces are relieved by twisting in opposite to the applied torsion without the formation of false twist, bringing about reversible torsional behavior.

Chapter 4. Strength prediction model of carbon nanotube yarns

4.1 Introduction

Since carbon nanotubes(CNTs) were found in 1991[69], many researchers expended much effort to reveal their remarkable mechanical and physical properties in large scale. As part of these efforts, CNT assemblies such as arrays, films and yarns(or fibers) have been fabricated and their properties have been investigated. Among them, the structure of CNT yarns is similar to that of staple yarns spun from short staple fibers when constituent CNTs are regarded as short fibers. CNT yarns are consisted of well aligned and highly packed CNTs, therefore, it have been expected that CNT yarns have more excellent properties than other assemblies and several research groups have studied the fabrication and performance of CNT yarns.[18-21]

CNT yarn manufacturing processes are classified into wet spinning method and dry spinning method. Wet spinning which is similar to the coagulation spinning fabricating conventional polymer fibers is the method of using CNT dispersion solution. Solution in which CNTs are well dispersed is extruded into another solution so that CNT agglomeration is created because dispersion system is destroyed by another solution. When CNTs are aggregated, the agglomeration in which CNTs are aligned have the form of a fibre of fibers induced by liquid flow. Vigolo et al.[24] introduced a simple method to assemble single-walled CNTs(SWCNTs) into long ribbons and

fibers. SWCNTs were dispersed in surfactant solutions and nanotubes were recondensed by polyvinylalcohol(PVA) solution. SWCNTs/PVA composites which features are ribbon or fiber are created by induced flow. However, PVA is non-conductive polymer so that SWCNTs/PVA fibers have low electrical and thermal conductivity[23] and removal a large amount of PVA is not easy task without maintenance fiber feature. Therefore, polymer-free processes have been developed by using acid dispersion. Ericson et al.[22] proposed the method dispersing SWCNTs in superacid. SWCNTs surrounded by acid anions are ordered into aligned phase, hence liquid crystal solution is created and then spun into coagulation solution such as diethyl ether, 5% sulfuric acid and water. Kozlov et al.[23] developed surfactant-stabilized nanotube dispersion, but introduced various acids(hydrochloric, sulfuric, nitric, and phosphoric) or bases(NaOH and KOH) as coagulation medium by using the knowledge that dispersed nanotubes is aggregated when the pH of a solution changes. From the polymer-free processes, pure CNT fibers could be obtained, however the chemical dispersing process leads to a low usage of CNTs and induces residual contamination of CNTs from the fluid. The resulting neat fiber has mechanical and physical properties much lower than individual CNTs, thus dry spinning methods were suggested as alternatives. Zhu et al.[26] proposed the method to synthesize long strands of ordered single-walled carbon nanotubes up to several centimeters directly by the catalytic chemical vapor deposition(CVD) technique with a floating catalyst method in a vertical furnace, where n-hexane is catalytically pyrolyzed. Li et al.[25] spun fibers of CNTs directly from the CVD synthesis zone of a furnace using a liquid source of carbon and nanocatalyst. An aerogel of nanotubes is captured and

wound out of the furnace hot zone continuously as a fiber or film while the liquid feedstock consisted of small quantities of ferrocene and thiophene mixed with hydrogen injected into hot zone. Ma et al.[61, 70] produced SWCNT fibers by twisting SWCNT films prepared by a floating catalyst CVD and the micromechanical process in SWCNT fibers and films is revealed by applying Raman tests to them. Meanwhile, CNT yarns could be produced by spinning from vertically aligned CNT arrays. Since Jiang et al.[27] firstly spun CNT yarns from CNT arrays, lots of efforts have been performed to improve the properties of CNT yarns. Zhang et al.[12] modified method by introducing twist during spinning of multiwalled CNTs(MWCNTs) from nanotube arrays and achieved yarn strengths greater than 460 megapascals by fabricating various yarn structures such as multi-ply yarns, knitted yarns, knotted yarns and PVA infiltrated yarns.

Although several efforts have been performed to improve physical properties of CNT yarns, they are still much lower than them of individual CNTs.[10-13] Thermal and electrical conductivity of CNT yarns are in the order of 100W/mK and 100S/cm which are one order less than them of CNTs. In the case of mechanical properties, there are significant differences compared to other properties. CNTs possess superb mechanical properties including elastic modulus and strength, ~1TPa and ~50GPa for multi-walled nanotubes, respectively, while modulus and strength of CNT yarns are in the order of 10GPa and 1GPa. For these reasons, theoretical analysis have been performed by several research groups. Beyerlein et al.[14] demonstrated relationship between Weibull strength CNTs and the statistical failure behavior of CNT yarns, i.e. statistical strength with surface twist angle,

number of CNTs in cross-section, and gauge length were predicted using Monte Carlo simulation. Vilatela et al.[15] considered deformation of cross-section of CNT bundles and concentrated on stress transfer mechanism based on the interfacial shear stress between CNTs, thus, CNT fiber strength were determined according to the nanotube length, shear strength and contract area between CNTs. Lu et al.[16] examined the interactions among CNTs in a yarn. They established the model regarding CNT entanglement as two connecting self-folded CNTs originated from the van der Waals interactions. It was demonstrated that tensile properties of CNT entanglements with geometrical condition such as CNT radius and length. Liu et al.[17] investigated the deformation and strength mechanism using coarse-grained molecular dynamics simulations. The fully atomistic CNT model was replaced by a line of beads connected via springs and van der Waals forces between the beads were considered. Stress–strain relationships of CNT fibers with failure mechanism were determined with the structural evolution mechanisms of CNT fibers under tension.

Although various models to predict mechanical properties were established as stated above, mechanical properties of CNT yarns developed in recent years is still lower compared to individual CNTs. Existing models supposed the geometry of CNT yarns treated in classical yarn theory or simplified that. In other words, there was lack of the consideration on the actual geometry of CNT yarns. In addition, CNT agglomerations could be created inside the yarn when gaps between CNTs become shorter than Van der Waals length(about 3.4Å). It is possible that the existence of agglomerations make CNT yarns non-uniform, thus, a new model should be needed to consider

them. In this study, at first, morphological study was performed to develop theoretical model. Geometrical deformation of CNT yarns were observed by using in-situ tensile test and focused ion beam milling of them was performed to investigate changes in inner structure. Then, through the information of geometries, failure mechanism was defined and theoretical model was built up in respect of interfacial shear stress originated from Van der Waals forces by developing new concept(CNT cluster) and frictional stresses due to the lateral pressure generated from inherent yarn structure. In these days, CNT yarns are recognized as most beneficial structure because of various and significant potentials to superelastic muscles, high strength and conductive fibers, field-emission electron sources, etc.[49, 71, 72] Understanding geometrical information during the deformation and their effect on the mechanical behavior would make applications of CNT yarns successful.

4.2 Experimental

4.2.1 In-situ tensile test

For the manipulation of CNT yarns in a nano-scaled displacement, nanomanipulator which consists of X,Y,Z stages(Sigma Koko, TSDS-252S, 253) and three piezoelectric actuators(New Focus, 8353-V) were assembled into the stages. Both ends of CNT yarn was fixed on manipulator and piezoelectric actuator using carbon tape, respectively. *In-situ* tensile test was operated by moving manipulator in scanning electron microscope(SEM, JEOL JSM-6390LV). Gauge length of CNT yarns was 350 μm and strain rate set as 3μm/min

4.2.2 Inner structure analysis

An FEI Nova 200 dual beam focused ion beam (FIB) system was used to investigate cross-sections through the fractured CNT yarns. The Ga+ ions in FIB were used and their intensity was controlled for shaping and finishing the cross-sections. No coatings were applied to the samples for FIB milling or SEM imaging. FIB milling processes were performed in parts depending on the distance from the fracture surface. Distances were set as ~100μm,~1mm and ~1cm.

4.3 Theoretical modeling

The inner structure of CNT yarns is composed of a core-sheath structure[43]. Packing density becomes higher from the sheath to the core due to the existence of lateral pressure of the yarn. Most of CNTs exists in the bundle, i.e. CNTs agglomerate together to form bundle by van der Waals interaction except for CNTs in the outermost regions. We focused on these bundles to develop a new model. Firstly, it is assumed that the stress transfer will occurs between CNT bundles, not between individual CNTs, when a load is applied to the CNT yarns. In addition, tension in CNT yarns are limited by friction, the contribution of transverse forces originated from the idealized helical yarn structure[52]. In other words, additional frictional forces occurs between CNT bundles when CNT yarns is under tension. Meanwhile, there are various structures of bundles in CNT yarns and structure of bundle should be determined to consider the region where interfacial sliding and friction occur. Thus, the concept of CNT cluster like as a unit cell consisting

of hexagonal closed packed CNTs in CNT bundle was introduced in new model.(see Figure 4-1)

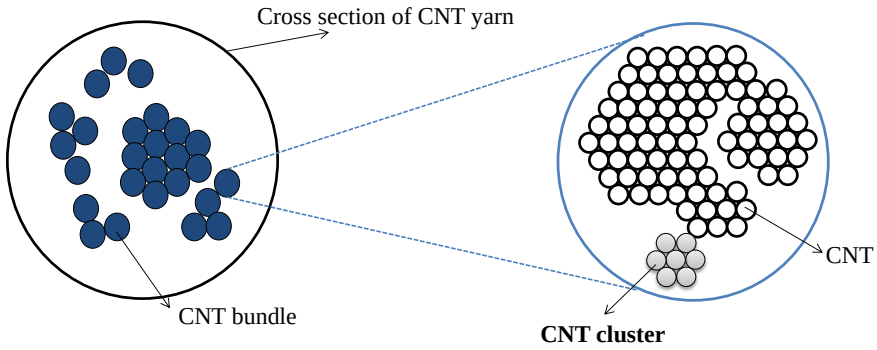

Figure 4-1. The concept of CNT cluster.

Each bundle is composed by CNT cluster and close packing of circular CNTs in hexagonal outline effect on the interfacial interaction. As bundle is consisted of bigger CNT clusters, the structure of bundle becomes coarser. With the 'CNT cluster' concept accepted, it is reasonable to conclude that the sum of interfacial shear strength generated from Van der Waals interaction and stresses calculated from friction originated from inherent yarn structure will determine the tensile strength of CNT yarns.

4.31 Interfacial shear strength based on Van der Waals interaction

Commercial molecular dynamics software(Material Studio® 5.5) by Accelrys to calculate the interfacial shear stress between bundles. Assuming that all

CNT bundles have hexagonal closed packed CNTs, i.e. CNT clusters in them, the number of CNTs and layers in each cluster can be predicted. It is assumed again that outmost CNTs in cluster involve the frictional load transfer between CNT bundles. Molecular dynamics is a powerful method to calculate the interfacial shear stress (τ) between CNT bundles, however a long computational time is unavoidable(a definite disadvantage). To reduce computational time, we simplified the geometrical model introducing cut off distance(12.5Å) ignoring the Van der Waal interaction with other CNTs which located further than the distance, thus only the three outer walls of MWNT was considered. Furthermore, because we treated MWNTs with diameter of about 15nm(the outermost wall has armchair structure(150,150)), numerous atoms should be considered. Therefore, CNT length was also simplified as 4.92Å , which is minimal length including hexagon consisted of carbon atoms. Considering assumptions stated above, the potential energy of all CNTs is calculated as adjacent CNTs in clusters, i.e. bundles move along the yarn direction or the tensile axis (see Figure 4-2), from which the interfacial shear stress is calculated by,

$$\tau = \frac{E}{\pi r L^2}\cos\alpha \qquad (1)$$

where r and L are the radius and length of individual CNT, respectively, while E is the variation of the potential energy caused by position change of CNT clusters in a twisted yarn. α is the helix angle on the yarn surface.

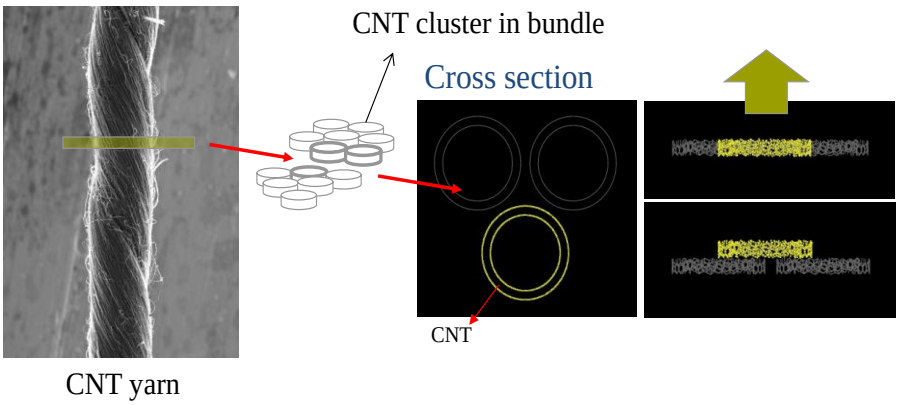

Figure 4-2. Molecular dynamics for calculating the interfacial shear stress between CNT clusters(bundles).

4.3.2 Frictional stress due to the lateral pressure in the yarn

CNT yarns are structurally very similar to staple yarns regarding CNTs as short staple fibers. To calculate frictional stresses between bundles inside yarn, we developed staple yarn theory presented by Hearle[52]. According to Hearle, the fibers are arranged in a helical assembly taking account of ideal migration. It is assumed that the fibers are perfectly elastic and follow Hooke's and Amonton's Laws. Considering development of frictional forces on a yarn element(see Figure 4-3), frictional stress is calculated by,

$$\tau = (\mu 2\pi a / \pi a^2)\int_0^s G(1-(2(s-q)/L_f)dq \qquad (2)$$

where μ is the frictional coefficient and a is the CNT radius. s is the length near the end of fiber in which slippage occurs. G in Equation 2 is the transverse stress(lateral pressure) given by:

$$G = E_{CNT}\varepsilon_y[\frac{1+\nu_{LT}}{(1+2\nu_{LT(CNT)})}\frac{c^2}{u^2}(1-u^{1+2\nu_{LT(CNT)}})-\nu_{LT}\frac{1-u^{2\nu_{LT(CNT)}-1}}{(2\nu_{LT(CNT)}-1)}] \quad (3)$$

where E_{CNT} is the modulus of CNT and ε_y is the yarn extension. ν_{LT} and $\nu_{LT(CNT)}$ are axial Poisson's ratio, i.e. (transverse strain/axial strain) for the yarn and CNT, respectively. ν_{LT} is function of the helix angle of fibers on the yarn surface originated from orientation distribution of constituent fibers and developed by Pan[35]. c and u are parameters introduced by the idealized helical yarn geometry. c is the value $\cos\alpha$, where α is the helix angle on the yarn surface and u is a radial position and varies from c at the center of the yarn and 1 at the surface.[52] q is the length gripped by transverse specific stress in s and L_f is the length of CNT. Thus, frictional stress is reduced by a factor $(1-(2(s-q)/L_f)$, the number 2 in the factor means that friction acts in opposite direction against tensile direction.

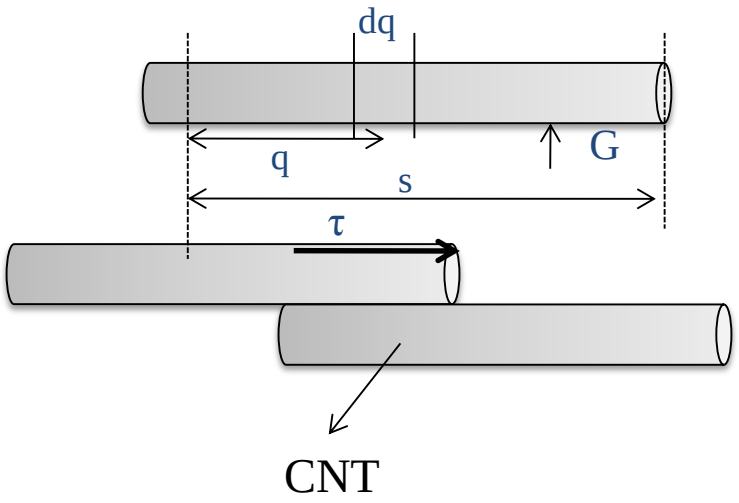

Figure 4-3. Stresses on a yarn element[31].

4.4 Results and discussion

Geometrical change of CNT yarns were observed by using in-situ tensile test to find out the failure mechanism.(see Figure 4-4) From the in-situ tensile test results, the failure process can be divided into three steps. In the first step(Figure Figure 4-4(a)), CNT yarns are extended in tensile direction ,while yarn is compressed transversely to the tensile direction(yarn diameter decreases) due to the Poisson's ratio. It is supposed that individual CNTs are stretched and oriented to the tensile direction in this step. In the second step(Figure 4-4 (b),(c) and (d)), necking occurs in CNT yarns. Before necking occurs, CNTs are partially compacted by filling in empty space inside the yarn, however this movement of CNTs is limited by the

entanglement. Thus, restriction on compaction makes various size of CNT bundles and bundling appears considerably in the place which the most entanglements existed. After bundles are created as a certain size, bundle does not develop their size and the compaction is over. CNT yarn is untwisted during bundling and compression process. In the final step(Figure 4-4 (e) and (f)), interbundle slippages are widespread and failure occurs. Individual CNTs are twisted and bent initially, however CNTs undergo untwisting while CNTs are bundled under yarn tension. As tensile stress increases, interbundle sliding occurs when tensile force overcomes weaken twisted forces and Van der Waals interaction.

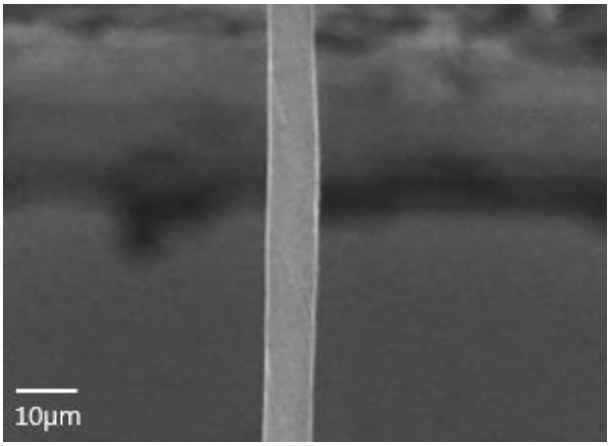

(a)

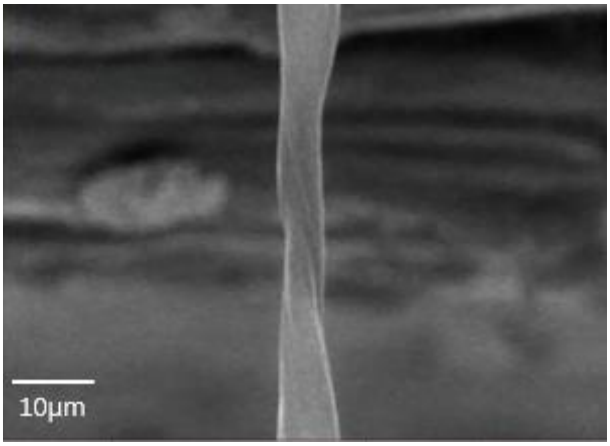

(b)

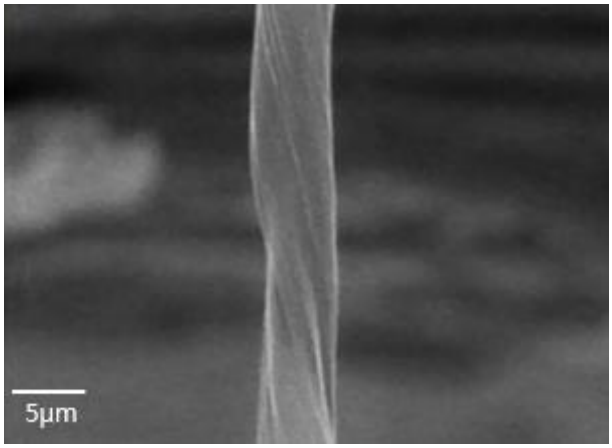

(c)

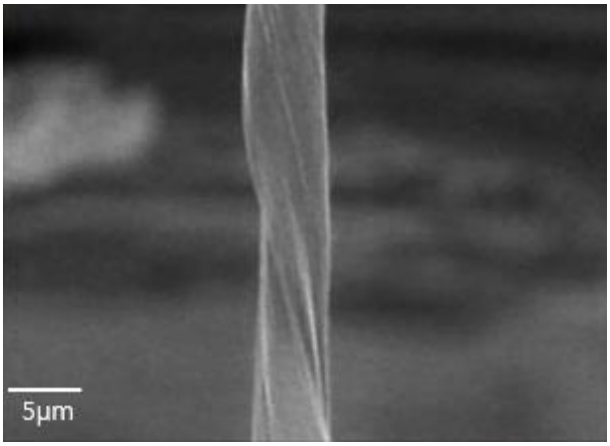

(d)

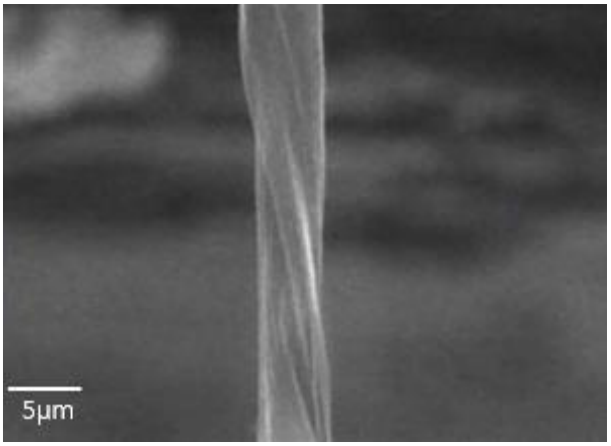

(e)

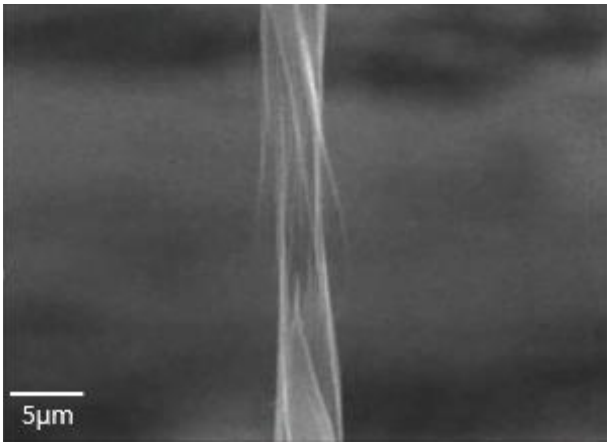

(f)

Figure 4-4. The SEM images of CNT yarns under different tensile strain at (a)1.56e^{-3}, (b)0.0137, (c)0.0148, (d)0.0166, (e)0.0239 and (f)0.0330.

Cross-sectional images(see Figure 4-5) obtained from FIB milling also provide the information related to the failure mechanism. The internal CNT

yarn structure without deformation is shown by Figure 4-5(a). There are many vacancies inside yarn and packing density becomes larger and larger from the surface to the center. Most of CNTs exist in a form of bundle, not individually. While tensile load applies to the CNT yarns and failure occurs, the inner structure changes drastically. There is little difference between the cross section images of the region which is few centimeter away from the fracture surface and the region without deformation.(see Figure 4-5(a) and (b)). However, as the region is located nearer fracture surface, vacancies inside the yarn become smaller. It means that compaction is concentrated on the place in which necking occurs and most of bundles are located close to each other just before fracture occurs.

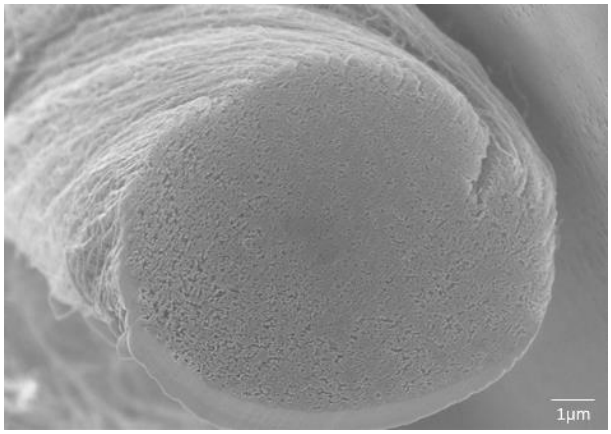

(a)

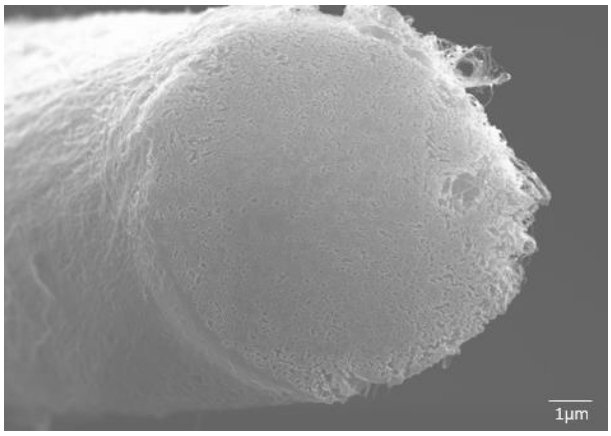

(b)

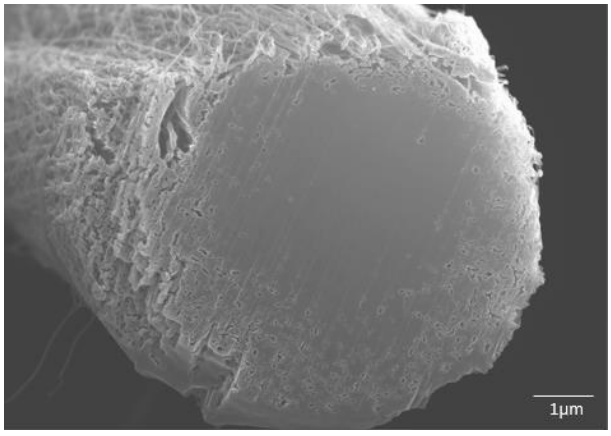

(c)

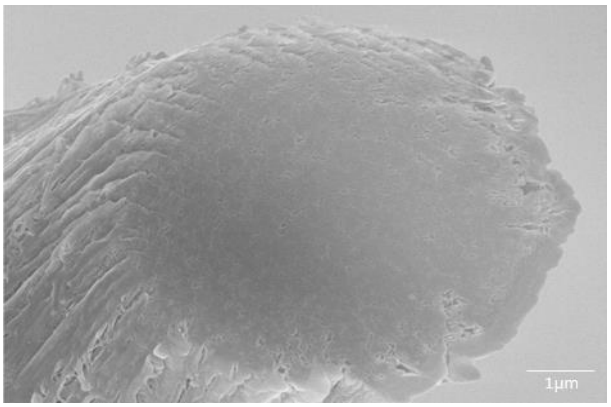

(d)

Figure 4-5. The SEM images of FIB sections milled through CNT yarns. (a) The cross-section of CNT yarn without deformation. Cross-sections of fractured CNT yarns were obtained at different parts depending on the distance from the fracture surface, (b) ~1cm, (c) ~1mm and (d) ~100μm.

From internal and external structural analysis results, a theoretical model was developed based on three assumptions: (1) Interfacial shear strength is determined by interbundle slippage which is exactly slippage between CNT clusters in bundles and the distance between clusters is 3.4Å, which is the equilibrium distance between two parallel nanotubes. (2) When failure occurs, there are no geometrical changes in CNTs. In other words, bundles without structural deformation, which are pulled out in the tensile direction, are considered. (3) The sum of interfacial shear strength and stresses calculated from frictional forces determines the tensile strength of CNT yarns.

Size of clusters, i.e. the number of CNTs in clusters was defined to calculate interfacial shear stress between bundles. The total number of CNTs in the CNT yarn was estimated from a relationship between yarn helix angle and fiber volume fraction in the same manner with Miao et al[37]. Density of CNT yarn was determined by weighing a 300mm length of yarn sample on a Mettler Toledo AX26DR Ultra Micro Balance and dividing yarn volume. Volume fraction of CNT yarns was calculated by dividing nanotube density of 2.1/cm^3[73]. The relationships of volume fraction with the yarn surface twist angle is presented in Figure 32. The total number of CNTs in the yarn was calculated using the following equation.

$$N_{\text{Total CNTs}} = V_f \frac{R^2\pi}{r^2\pi} \quad (4)$$

where r is the radius of individual CNTs, while R and V_f are the radius and fiber volume fraction of CNT yarns, respectively. The radii of CNT and CNT yarns which treated in this study were measured to be 15nm and 5μm, respectively. The length of CNT was measured as about 150μm. The total number of CNTs in the yarn could be then estimated from 12300 to 125223 depending on surface angle(see Figure 4-6). The number of CNTs in cluster and CNTs in which effect on the interfacial shear stress among them were considered based on two assumptions. First, number of CNTs in cluster is proportional to their cross sectional area. As number of CNTs in clusters decreases more and more, number of clusters increases. Second, CNTs in each cluster are hexagonal closed packed without geometrical deformation. In this case, close packing of circular CNTs in hexagonal outline only effect on the interfacial shear stress(see Figure 4-7).

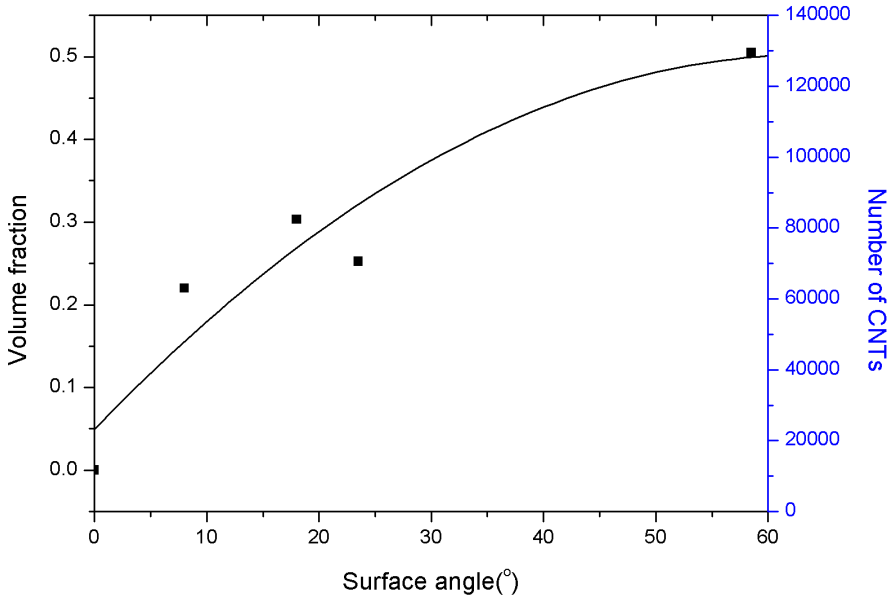

Figure 4-6. The effect of yarn surface angle on the volume fraction and total number of CNTs which is estimated from equation 4.

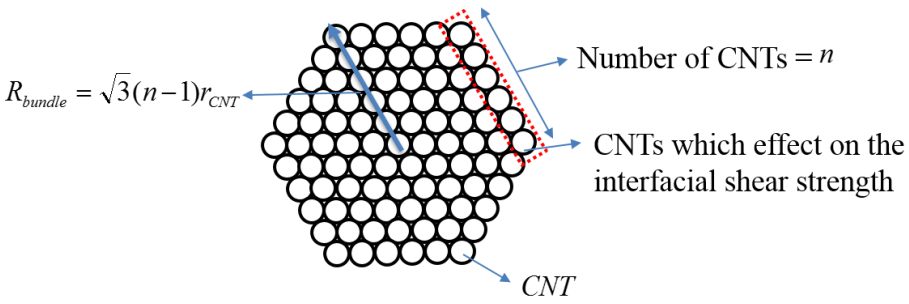

Figure 4-7. Hexagonally close-packed cluster.

Note that strength is determined as lowest value so that only one hexagonal outline was considered in this study, although clusters have total 6 outlines. Meanwhile, a molecular dynamics simulation was carried out to compute a variation of potential energy when a CNT was pulled away against adjacent two CNTs in the axial direction of yarn. The energy difference was calculated to be 47.93Kcal/mol for multi-walled CNTs with a diameter of 15 nm. As the number of adjacent CNTs increased, the energy variation was also calculated when again a CNT was pulled away against increased adjacent CNTs. As expected, the potential energy increases linearly as the number of adjacent CNTs increases (see Figure 4-8).

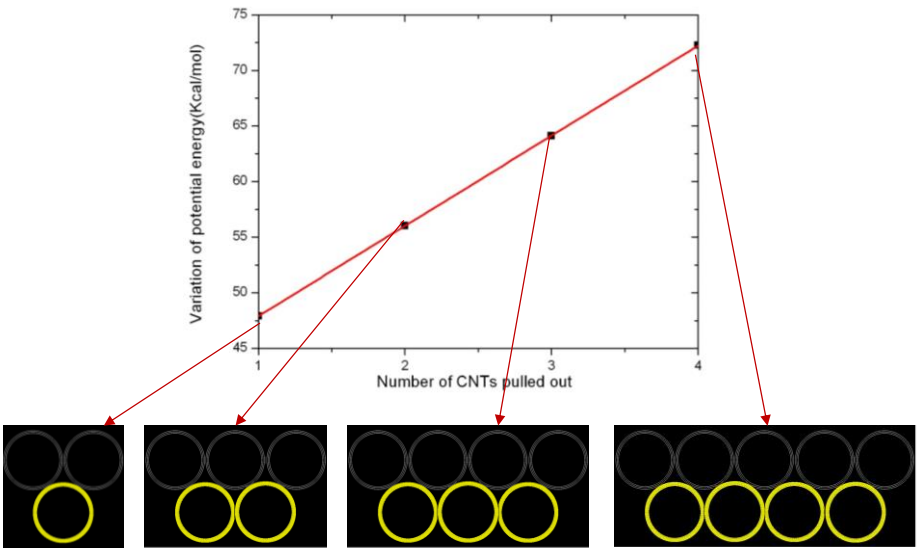

Figure 4-8. A variation in the potential energy as the CNTs were pulled out of their assembly.

Interfacial shear stress between CNT clusters in CNT yarn was predicted using the morphological information on CNT yarn and the pull-out simulation results above as shown in Figure 4-9(a) and (b). Note that actual size of CNT cluster, i.e. the number of CNTs in the cluster was not determined exactly at the moment; thereby predicted interfacial shear stress of CNT yarns was provided with a function of it. The number of CNTs in cluster determines the development of bundle. As bundling occurs and develops more and more, size of cluster decreases largely. In other words, growth of bundle reduce interfacial shear strength. Total number of CNTs is different depending on surface angle so that maximum interfacial shear

stress is limited by total number of CNTs. For example, number of CNTs in CNT clusters does not exceed 44979 when surface angle of yarn is 10°. From the theory, when it can be claimed that CNT bundles consisting of approximately 20,000 CNTs mainly exist inside the CNT yarn, interfacial shear stress was calculated from 404.74MPa to 809.48MPa according as surface angle changes from 0° to 60°(see Figure 4-9(b)).

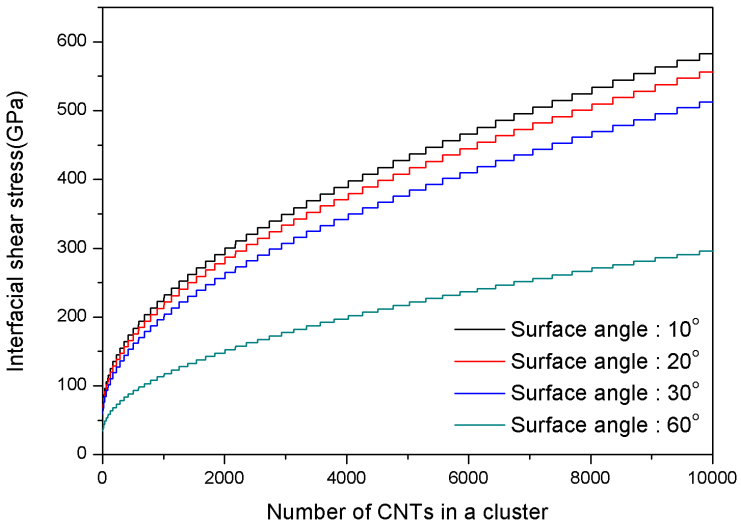

(a)

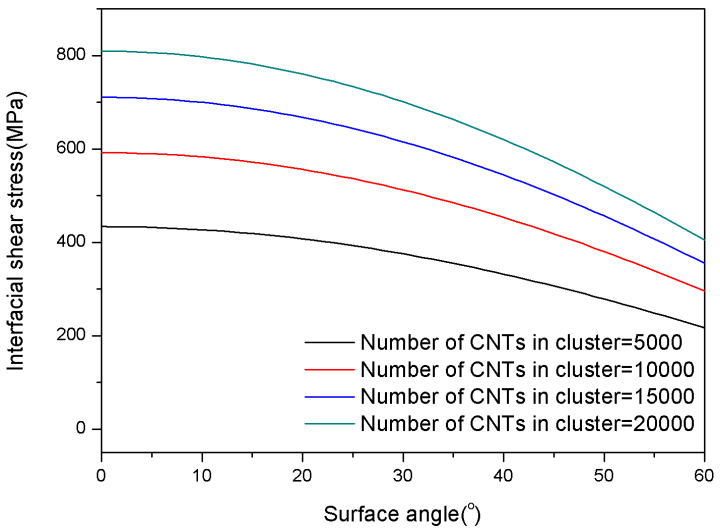

(b)

Figure 4-9. Predicted interfacial shear strength of CNT yarn. (a) according to the size of CNT cluster and (b) according to the surface angle.

Frictional stress was calculated by equation 2 and 3. At first, s which is slippage length was set as 4.92Å which is same value used in interfacial shear strength calculation. Frictional coefficient, μ was investigated as about 0.9 for vertically aligned CNTs[42]. E_{CNT} and $\nu_{LT(CNT)}$ was calculated as 1TPa and 0.2 by structural mechanics approach for the analysis of CNTs, respectively[74]. ε_y was calculated as 0.05 from our tensile test results. Frictional stress was calculated as Figure 4-10.

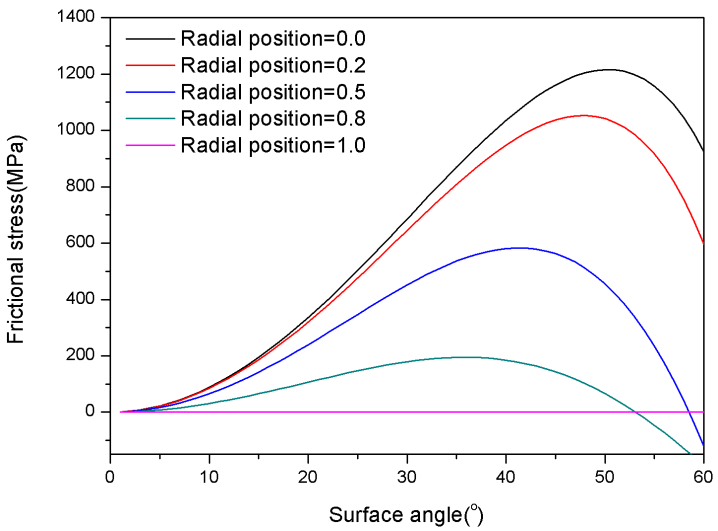

Figure 4-10. Predicted frictional stress in CNT yarn according to the radial position.

Note that radial position varies from 0 at the center of the yarn and 1 at the surface. Generally, frictional stress increases as surface angle increases,

since transverse stress increases as degree of twist increases. However, increment of frictional stress is limited due to the difference of Poisson's ratio between yarn and individual fibers. In this case, Poisson's ratio of CNT is only 0.2, however Poisson's ratio of yarn was calculated from 0.69 to 0.72 according as surface angle changes from 0° to 60°, i.e. Poisson's ratio of yarn is about three times larger than that of CNT(see Figure 4-11).

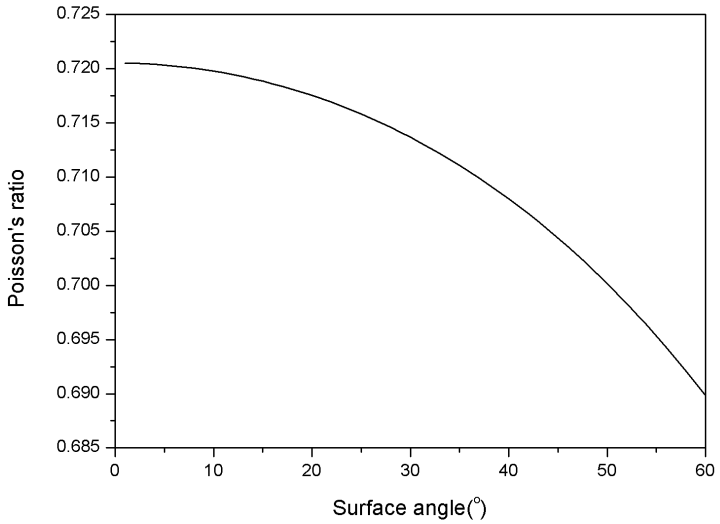

Figure 4-11. Axial Poisson's ratio of CNT yarns according to the yarn surface angle.

Note that when twist goes up, yarn structure will be tighter, transverse strains of the yarn due to longitudinal strain decreases. Yarn tried to contract in transverse direction when it strained, while individual CNTs are not easy to shrink due to the low Poisson's ratio. Therefore, the direction of

transverse stress was changed, finally the stress was applied in opposite direction. This decrement of frictional stress occurs as radial position is closed to the surface region and the effect of frictional stress disappears completely at the surface. Finally, the tensile strength of CNT yarns was calculated by summation of interfacial shear stress and frictional stress(see Figure 4-12).

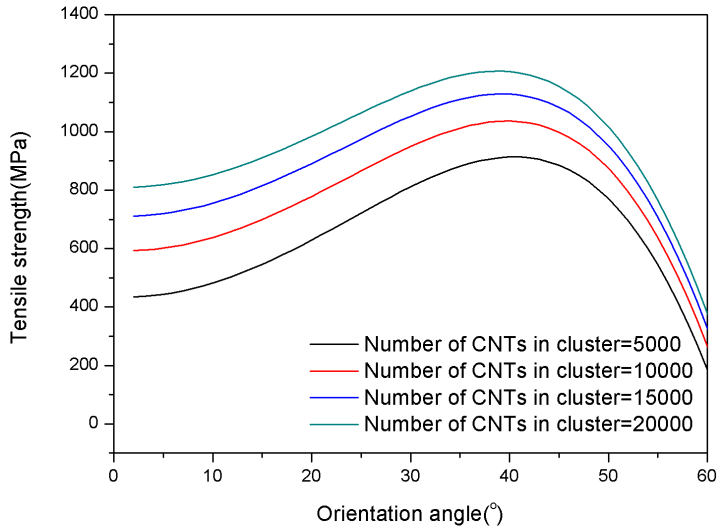

(a)

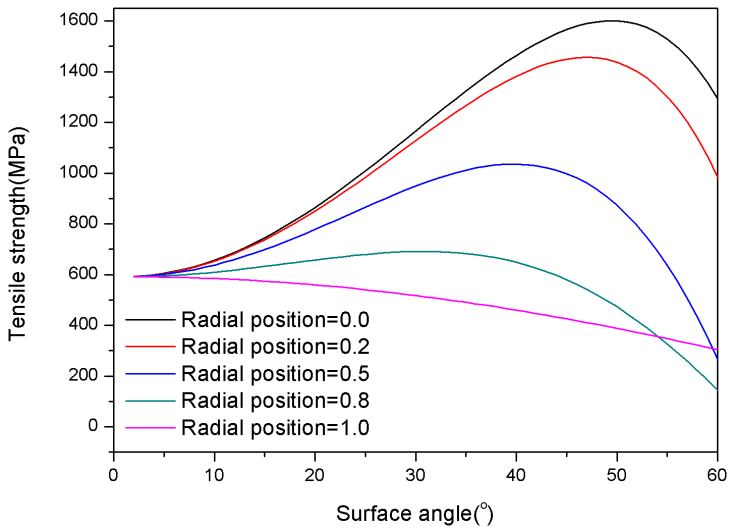

(b)

Figure 4-12. The tensile strength of CNT yarns (a) depending on the number of CNTs in the bundle when radial position is 0.5 and (b) depending on the radial position when the number of CNTs is 10,000.

The tensile strength increases as the number of CNTs in cluster increases because CNTs which effect on the interfacial shear stress increases. (see Figure 4-12(a)) According to the increment of interfacial shear stress, the influence of frictional stress is relatively reduced so that maximum strength value with respect to the orientation angle decreases. The number of CNTs in cluster is physically associated with the strain rate during tensile test. As strain rate increases, it is not sufficient to develop the inner structure exquisitely, i.e. close packing of circular CNTs in hexagonal outline increases, thus strength increases. Meanwhile, tensile strength highly depends on the radial position which failure occurs, since transverse stress are depended on radial position(see Figure 4-12(b)). When surface angle is 0, there is no the effect of transverse stress and only interfacial shear stress originated from Van der Waals exists. Therefore, tensile strength increases from maximum interfacial shear strength value and then decreases again according to the tendency of changes in transverse stress as surface angle changes from 0° to 60°. In other words, tensile strength increases as radial position is closed to the center, since the effect of friction increases largely. However, it is impossible that fracture occur in the center region, because CNTs are highly packed during yarn spinning process. From the image which we obtained from FIB milling, failure mechanism occurs in the region which radial position is larger than about 0.5 and it is expected that the development of bundle and intersliding appear in this part. Considering the influence of the number of CNTs in cluster and radial position, tensile strength was predicted by comparing with experimental values depending on the yarn surface angle(see Figure 4-13).

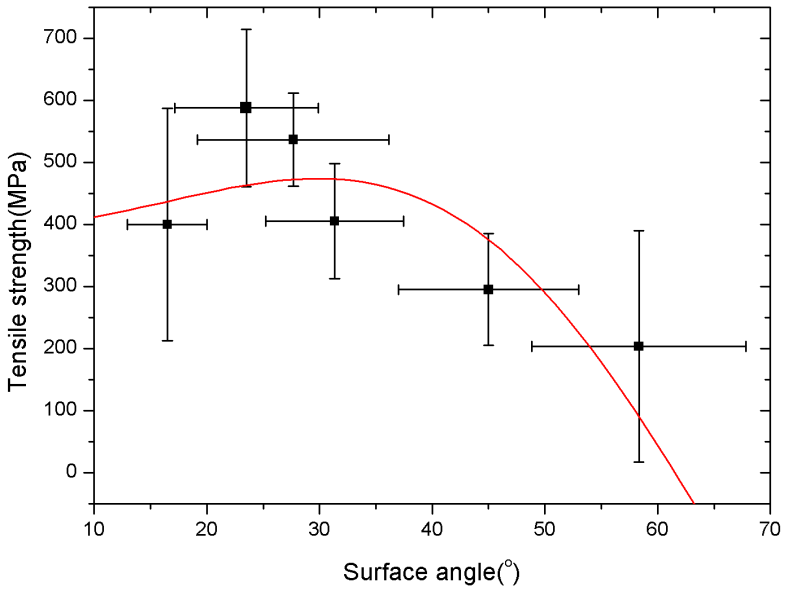

Figure 4-13. Predicted tensile strength of CNT yarns according to the yarn surface angle. The comparison of predicted results using a measured experimental results which is represented as points with x and y error bar. Radial position and the number of CNTs in cluster were set as 0.85 and 4000, respectively.

In this prediction, Radial position and the number of CNTs in cluster were set as 0.85 and 4000, respectively. Note that in case of very low twisted yarn(surface angle is lower than 20°), tensile strength was measured with high standard variation, due to lack of the cohesion between individual CNTs. Tensile strength appears highest values when surface angle is near the value, 25° and the tendency of changes in strength depending on surface angle is accordance with predicted values. According to this new model, strength can be increased in respect of interfacial shear stress and frictional stress. First, the development of CNT bundle should be avoided. If bundling

under tension is reduced, inner structure of bundle remains coarse, so region in which intersliding occurs will be increased. Second, the effect of frictional force should be increases. CNTs near the center region should exist individually, thus many CNTs or bundles should be contributed to the failure mechanism.

4.5 Conclusion

To predict the tensile strength of CNT yarns, deformation of CNT yarns was observed by using in-situ tensile test and the changes in inner structures were investigated by FIB milling process. Based on the experimental results, failure mechanism was defined and theoretical model was built up in respect of interfacial shear stress originated from Van der Waals forces and frictional stresses due to the lateral pressure generated from inherent yarn structure. A new concept, CNT clusters which divides CNT bundles like as unit cell and have hexagonal packed structure was introduced to define the model. Assuming that close packing of circular CNTs in hexagonal outline only effect on the interfacial shear stress, the effect of Van der Waals forces was considered in the model. Meanwhile, classical yarn theory was adopted to investigate the structure effect of the yarn. With the 'CNT cluster' concept accepted, the strength of CNT yarns was predicted by combine interfacial shear stress and frictional stress. The influence of the number of CNT cluster which reflects the inner structure of CNT bundle and radial position in which fracture occurs on tensile strength was investigated. Finally, the method to improve tensile strength was proposed based on theoretical model.

Chapter 5. Concluding remarks

Based on the knowledge of the classical staple yarn theories and internal structure analysis, the strength of CNT yarns was predicted by introducing a new model considering Van der Waals interaction among individual CNTs.

At first, strength of CNT yarns was predicted from two previous yarn theories to investigate the difference between staple yarns and nanoscale CNT yarns. The statistical strength of CNT yarn was investigated using staple yarn theory developed by Pan. Introducing some parameters such as Young's modulus of CNT, frictional coefficient between CNTs and Weibull parameters representing stochastic strength of CNTs to the model, the statistical strength was calculated considering the potential function in molecular dynamics(MD) to develop the effect of inter-CNT friction. According to the short fiber theory, individual CNTs have to carry external force equally, however the existence of CNT agglomerate depending on the radial position, crimped and misaligned CNTs disturbed accurate prediction. Thus, the actual measurement is two orders of magnitude lower than we predicted. Next, strength of CNT yarns was predicted from the theory of the mechanics of staple fiber yarns introduced by Hearle. For a given external force, the response of a yarn element such as the resultant deformation, the internal stresses and strains was calculated. Considering occurrences of inter-CNT slippage, yarn strength was predicted similar to the experimental values as long as slippage length is equal to the length of CNT. Thus, it was concluded that the major failure mechanism is highly depended on the inter-

CNT slippage.

The mechanical behavior of CNT yarns was investigated using *in-situ* polarized Raman spectroscopy. For investigating tensile behavior, changes in the orientation distribution function(ODF) and Raman band shift were examined at different strain levels using different diameter yarns. It was concluded that CNTs in the center receive tension continuously, but CNTs in the surface get tension only at low strain. CNT bundles, which are highly compacted CNTs caused by Van der Waals interaction, were created when CNT yarn is tensioned. In addition, the torsional behavior of CNT yarns was investigated according to the boundary conditions, which are one-end tethered and two-end tethered conditions. Changes in the ODF and Raman band shift were examined during untwisting and re-twisting process. It was found that in case of one-end tethered yarns, false twist and permanent deformation occur, results in irreversible torsional behavior. In case of two-end tethered yarns, high torque forces are relieved by twisting in opposite to the applied torsion without the formation of false twist, bringing about reversible torsional behavior.

Based on the result of chapter 2 and chapter 3, a new model predicting strength of CNT yarns was established. In order to create the more precise model, deformation of CNT yarns was observed by using in-situ tensile test and the changes in inner structures were investigated by FIB milling process. Based on the experimental results, failure mechanism was defined and theoretical model was built up in respect of interfacial shear stress originated from Van der Waals forces and frictional stresses due to the lateral pressure

generated from inherent yarn structure. A new concept, CNT clusters which divides CNT bundles like as unit cell and have hexagonal packed structure was introduced to define the model. Assuming that close packing of circular CNTs in hexagonal outline only effect on the interfacial shear stress, the effect of Van der Waals forces was considered in the model. Meanwhile, classical yarn theory was adopted to investigate the structure effect of the yarn. The influence of the number of CNT cluster which reflects the inner structure of CNT bundle and radial position in which fracture occurs on tensile strength was investigated.

In conclusion, there are two strategies for improving the tensile strength of CNT yarn. First, interface between individual CNTs should be enhanced, since the major failure mechanism is inter-bundle slippage. Indeed, several studies in respect of the enhancement of the interface have been investigated. However, the maximum strength of CNT yarns is no more than about 2.5GPa, when the interface was enhanced by covalent crosslinks between CNTs. The strength value is still one-order lower than predicted value by the classical staple yarn theories. From the result of in-situ Raman test, it was concluded that the bundling of CNTs in yarns should be avoided such that they can carry external force individually for high strength yarn. In other words, Van der Waals interaction between CNTs should be reduced and research on this method will be proceeded.

References

[1] McEuen PL, Fuhrer MS, Park H. Single-walled carbon nanotube electronics. Nanotechnology, IEEE Transactions on. 2002;1(1):78-85.

[2] Gao B, Chen YF, Fuhrer MS, Glattli DC, Bachtold A. Four-Point Resistance of Individual Single-Wall Carbon Nanotubes. Physical Review Letters. 2005;95(19):196802.

[3] Bachtold A, Henny M, Terrier C, Strunk C, Schönenberger C, Salvetat J-P, et al. Contacting carbon nanotubes selectively with low-ohmic contacts for four-probe electric measurements. Applied Physics Letters. 1998;73(2):274-6.

[4] Berger C, Yi Y, Wang ZL, de Heer WA. Multiwalled carbon nanotubes are ballistic conductors at room temperature. Appl Phys A. 2002;74(3):363-5.

[5] Hone J, Whitney M, Piskoti C, Zettl A. Thermal conductivity of single-walled carbon nanotubes. Physical Review B. 1999;59(4):R2514-R6.

[6] Kim P, Shi L, Majumdar A, McEuen PL. Thermal Transport Measurements of Individual Multiwalled Nanotubes. Physical Review Letters. 2001;87(21):215502.

[7] Demczyk BG, Wang YM, Cumings J, Hetman M, Han W, Zettl A, et al. Direct mechanical measurement of the tensile strength and elastic modulus of multiwalled carbon nanotubes. Materials Science and Engineering: A. 2002;334(1-2):173-8.

[8] Bellucci S. Carbon nanotubes: physics and applications. physica status solidi (c). 2005;2(1):34-47.

[9] Yu M-F, Lourie O, Dyer MJ, Moloni K, Kelly TF, Ruoff RS. Strength and Breaking Mechanism of Multiwalled Carbon Nanotubes Under

Tensile Load. Science. 2000;287(5453):637-40.
[10] Aliev AE, Lima MH, Silverman EM, Baughman RH. Thermal conductivity of multi-walled carbon nanotube sheets: radiation losses and quenching of phonon modes. Nanotechnology. 2010;21(3):035709.
[11] Atkinson KR, Hawkins SC, Huynh C, Skourtis C, Dai J, Zhang M, et al. Multifunctional carbon nanotube yarns and transparent sheets: Fabrication, properties, and applications. Physica B: Condensed Matter. 2007;394(2):339-43.
[12] Zhang M, Atkinson KR, Baughman RH. Multifunctional Carbon Nanotube Yarns by Downsizing an Ancient Technology. Science. 2004;306(5700):1358-61.
[13] Zhang X, Jiang K, Feng C, Liu P, Zhang L, Kong J, et al. Spinning and Processing Continuous Yarns from 4-Inch Wafer Scale Super-Aligned Carbon Nanotube Arrays. Advanced Materials. 2006;18(12):1505-10.
[14] Beyerlein IJ, Porwal PK, Zhu YT, Hu K, Xu XF. Scale and twist effects on the strength of nanostructured yarns and reinforced composites. Nanotechnology. 2009;20(48):485702.
[15] Vilatela JJ, Windle AH. Yarn-Like Carbon Nanotube Fibers. Advanced Materials. 2010;22(44):4959-63.
[16] Lu W, Chou T-W. Analysis of the entanglements in carbon nanotube fibers using a self-folded nanotube model. Journal of the Mechanics and Physics of Solids. 2011;59(3):511-24.
[17] Liu X, Lu W, Ayala OM, Wang L-P, Karlsson AM, Yang Q, et al. Microstructural evolution of carbon nanotube fibers: deformation and strength mechanism. Nanoscale. 2013;5(5):2002-8.
[18] Behabtu N, Green MJ, Pasquali M. Carbon nanotube-based neat fibers. Nano Today. 2008;3(5-6):24-34.
[19] Chou T-W, Gao L, Thostenson ET, Zhang Z, Byun J-H. An assessment of the science and technology of carbon nanotube-based

fibers and composites. Composites Science and Technology. 2010;70(1):1-19.
[20] Liu L, Ma W, Zhang Z. Macroscopic Carbon Nanotube Assemblies: Preparation, Properties, and Potential Applications. Small. 2011;7(11):1504-20.
[21] Lu W, Zu M, Byun J-H, Kim B-S, Chou T-W. State of the Art of Carbon Nanotube Fibers: Opportunities and Challenges. Advanced Materials. 2012;24(14):1805-33.
[22] Ericson LM, Fan H, Peng H, Davis VA, Zhou W, Sulpizio J, et al. Macroscopic, Neat, Single-Walled Carbon Nanotube Fibers. Science. 2004;305(5689):1447-50.
[23] Kozlov ME, Capps RC, Sampson WM, Ebron VH, Ferraris JP, Baughman RH. Spinning Solid and Hollow Polymer-Free Carbon Nanotube Fibers. Advanced Materials. 2005;17(5):614-7.
[24] Vigolo B, Pénicaud A, Coulon C, Sauder C, Pailler R, Journet C, et al. Macroscopic Fibers and Ribbons of Oriented Carbon Nanotubes. Science. 2000;290(5495):1331-4.
[25] Li Y-L, Kinloch IA, Windle AH. Direct Spinning of Carbon Nanotube Fibers from Chemical Vapor Deposition Synthesis. Science. 2004;304(5668):276-8.
[26] Zhu HW, Xu CL, Wu DH, Wei BQ, Vajtai R, Ajayan PM. Direct Synthesis of Long Single-Walled Carbon Nanotube Strands. Science. 2002;296(5569):884-6.
[27] Jiang K, Li Q, Fan S. Nanotechnology: Spinning continuous carbon nanotube yarns. Nature. 2002;419(6909):801-.
[28] Yu M-F, Files BS, Arepalli S, Ruoff RS. Tensile Loading of Ropes of Single Wall Carbon Nanotubes and their Mechanical Properties. Physical Review Letters. 2000;84(24):5552-5.
[29] Peng B, Locascio M, Zapol P, Li S, Mielke SL, Schatz GC, et al. Measurements of near-ultimate strength for multiwalled carbon

nanotubes and irradiation-induced crosslinking improvements. Nat Nano. 2008;3(10):626-31.
[30] Pan N. Prediction of statistical strengths of twisted fibre structures. Journal of Materials Science. 1993;28(22):6107-14.
[31] Hearle JWS, Grosberg P, Backer S. Structural mechanics of fibers, yarns, and fabrics. New York: Wiley-Interscience; 1969.
[32] Cox HL. The elasticity and strength of paper and other fibrous materials. British Journal of Applied Physics. 1952;3(3):72-9.
[33] Pierce; FT, B.Sc;, F.Inst.P. 32—X.—Tensile Tests for Cotton Yarns v.—"The Weakest Link" Theorems on the Strength of Long and of Composite Specimens. Journal of the Textile Institute Transactions. 1926;17(7):T355-T68.
[34] Daniels HE. The statistical theory of the strength of bundles of threads. I. Proceedings of the Royal Society of London Series A Mathematical and Physical Sciences. 1945;183(995):405-35.
[35] Pan N. Development of a constitutive theory for short fiber yarns : mechanics of staple yarn without slippage effect. Anglais. 1992;62(12):749-65.
[36] Kelly A, Macmillan NH. Strong Solids, 3rd Edn Oxford: Oxford University Press 1986.
[37] Miao M. Electrical conductivity of pure carbon nanotube yarns. Carbon. 2011;49(12):3755-61.
[38] Barber AH, Kaplan-Ashiri I, Cohen SR, Tenne R, Wagner HD. Stochastic strength of nanotubes: An appraisal of available data. Composites Science and Technology. 2005;65(15-16):2380-4.
[39] Kaplan-Ashiri I, Cohen SR, Gartsman K, Ivanovskaya V, Heine T, Seifert G, et al. On the mechanical behavior of WS2 nanotubes under axial tension and compression. Proceedings of the National Academy of Sciences of the United States of America. 2006;103(3):523-8.
[40] Barber AH, Andrews R, Schadler LS, Daniel Wagner H. On the

tensile strength distribution of multiwalled carbon nanotubes. Applied Physics Letters. 2005;87(20):203106--3.
[41] Li C, Chou T-W. A structural mechanics approach for the analysis of carbon nanotubes. International Journal of Solids and Structures. 2003;40(10):2487-99.
[42] Dickrell PL, Sinnott SB, Hahn DW, Raravikar NR, Schadler LS, Ajayan PM, et al. Frictional anisotropy of oriented carbon nanotube surfaces. Tribol Lett. 2005;18(1):59-62.
[43] Sears K, Skourtis C, Atkinson K, Finn N, Humphries W. Focused ion beam milling of carbon nanotube yarns to study the relationship between structure and strength. Carbon. 2010;48(15):4450-6.
[44] Mora RJ, Vilatela JJ, Windle AH. Properties of composites of carbon nanotube fibres. Composites Science and Technology. 2009;69(10):1558-63.
[45] Dalton AB, Collins S, Munoz E, Razal JM, Ebron VH, Ferraris JP, et al. Super-tough carbon-nanotube fibres. Nature. 2003;423(6941):703-.
[46] Xiao L, Liu P, Liang L, Jiang K, Feng X, Wei Y, et al. Barium-functionalized multiwalled carbon nanotube yarns as low-work-function thermionic cathodes. Applied Physics Letters. 2008;92(15):153108--3.
[47] Zhang S, Ji C, Bian Z, Yu P, Zhang L, Liu D, et al. Porous, Platinum Nanoparticle-Adsorbed Carbon Nanotube Yarns for Efficient Fiber Solar Cells. ACS Nano. 2012;6(8):7191-8.
[48] Zhao H, Zhang Y, Bradford PD, Zhou Q, Jia Q, Yuan F-G, et al. Carbon nanotube yarn strain sensors. Nanotechnology. 2010;21(30):305502.
[49] Foroughi J, Spinks GM, Wallace GG, Oh J, Kozlov ME, Fang S, et al. Torsional Carbon Nanotube Artificial Muscles. Science. 2011;334(6055):494-7.
[50] Ajayan PM, Stephan O, Colliex C, Trauth D. Aligned Carbon Nanotube Arrays Formed by Cutting a Polymer Resin—Nanotube

Composite. Science. 1994;265(5176):1212-4.
[51] Gommans HH, Alldredge JW, Tashiro H, Park J, Magnuson J, Rinzler AG. Fibers of aligned single-walled carbon nanotubes: Polarized Raman spectroscopy. Journal of Applied Physics. 2000;88(5):2509-14.
[52] Hearle JWS, Grosberg P, Backer S. Structural mechanics of fibers, yarns, and fabrics: Wiley-Interscience; 1969.
[53] Dresselhaus MS, Dresselhaus G, Saito R, Jorio A. Raman spectroscopy of carbon nanotubes. Physics Reports. 2005;409(2):47-99.
[54] Kuzmany H, Plank W, Hulman M, Kramberger C, Grüneis A, Pichler T, et al. Determination of SWCNT diameters from the Raman response of the radial breathing mode. Eur Phys J B. 2001;22(3):307-20.
[55] Tan P, Tang Y, Hu C, Li F, Wei Y, Cheng H. Identification of the conducting category of individual carbon nanotubes from Stokes and anti-Stokes Raman scattering. Physical Review B. 2000;62(8):5186-90.
[56] O'Connell MJ, Bachilo SM, Huffman CB, Moore VC, Strano MS, Haroz EH, et al. Band Gap Fluorescence from Individual Single-Walled Carbon Nanotubes. Science. 2002;297(5581):593-6.
[57] Liu T, Kumar S. Quantitative characterization of SWNT orientation by polarized Raman spectroscopy. Chemical Physics Letters. 2003;378(3-4):257-62.
[58] Hwang J, Gommans HH, Ugawa A, Tashiro H, Haggenmueller R, Winey KI, et al. Polarized spectroscopy of aligned single-wall carbon nanotubes. Journal Name: Physical Review B; Journal Volume: 62; Journal Issue: 20; Other Information: Othernumber: PRBMDO000062000020R13310000001; R14044PRB; PBD: 15 Nov 2000. 2000:Medium: X; Size: page(s) R13310-R3.
[59] Zhao Q, Wagner HD. Raman spectroscopy of carbon-nanotube-

based composites. Philosophical Transactions of the Royal Society of London Series A: Mathematical, Physical and Engineering Sciences. 2004;362(1824):2407-24.
[60] Cronin SB, Swan AK, Ünlü MS, Goldberg BB, Dresselhaus MS, Tinkham M. Resonant Raman spectroscopy of individual metallic and semiconducting single-wall carbon nanotubes under uniaxial strain. Physical Review B. 2005;72(3):035425.
[61] Ma W, Song L, Yang R, Zhang T, Zhao Y, Sun L, et al. Directly Synthesized Strong, Highly Conducting, Transparent Single-Walled Carbon Nanotube Films. Nano Letters. 2007;7(8):2307-11.
[62] Liu L, Barber AH, Nuriel S, Wagner HD. Mechanical Properties of Functionalized Single-Walled Carbon-Nanotube/Poly(vinyl alcohol) Nanocomposites. Advanced Functional Materials. 2005;15(6):975-80.
[63] Zhao Q, Daniel Wagner H. Two-dimensional strain mapping in model fiber-polymer composites using nanotube Raman sensing. Composites Part A: Applied Science and Manufacturing. 2003;34(12):1219-25.
[64] Lourie O, Wagner HD. Evaluation of Young's Modulus of Carbon Nanotubes by Micro-Raman Spectroscopy. Journal of Materials Research. 1998;13(09):2418-22.
[65] van Gurp M. The use of rotation matrices in the mathematical description of molecular orientations in polymers. Colloid & Polymer Science. 1995;273(7):607-25.
[66] van Gurp M. Letter to the Editor: On the use of spherical tensors and the maximum entropy method to obtain closure for anisotropic liquids. Journal of Rheology (1978-present). 1998;42(5):1269-71.
[67] Hearle JWS, Yegin AE. 33—THE SNARLING OF HIGHLY TWISTED MONOFILAMENTS. PART II: CYLINDRICAL SNARLING. Journal of The Textile Institute. 1972;63(9):490-501.
[68] Guo W, Liu C, Zhao F, Sun X, Yang Z, Chen T, et al. A Novel

Electromechanical Actuation Mechanism of a Carbon Nanotube Fiber. Advanced Materials. 2012;24(39):5379-84.
[69] Iijima S. Helical microtubules of graphitic carbon. Nature. 1991;354(6348):56-8.
[70] Ma W, Liu L, Yang R, Zhang T, Zhang Z, Song L, et al. Monitoring a Micromechanical Process in Macroscale Carbon Nanotube Films and Fibers. Advanced Materials. 2009;21(5):603-8.
[71] Jiang K, Wang J, Li Q, Liu L, Liu C, Fan S. Superaligned Carbon Nanotube Arrays, Films, and Yarns: A Road to Applications. Advanced Materials. 2011;23(9):1154-61.
[72] Wei Y, Weng D, Yang Y, Zhang X, Jiang K, Liu L, et al. Efficient fabrication of field electron emitters from the multiwalled carbon nanotube yarns. Applied Physics Letters. 2006;89(6):063101-3.
[73] Lu Q, Keskar G, Ciocan R, Rao R, Mathur RB, Rao AM, et al. Determination of Carbon Nanotube Density by Gradient Sedimentation. The Journal of Physical Chemistry B. 2006;110(48):24371-6.
[74] Xiao JR, Gama BA, Gillespie Jr JW. An analytical molecular structural mechanics model for the mechanical properties of carbon nanotubes. International Journal of Solids and Structures. 2005;42(11-12):3075-92.

Korean Abstract

매우 우수한 탄소나노튜브의 물성을 거시적인 스케일에서 응용하기 위해 탄소나노튜브실이 많은 연구 그룹들에 의해 제조되고 연구되어 왔다. 탄소나노튜브실을 다양한 응용 분야에 이용하기 위해서는 실 내부를 구성하는 탄소나노튜브의 기하학적 배향과 외부 응력에 대한 변형을 이해하는 것이 필수적이다. 그 중에서도 이 논문은 내부구조 분석을 바탕으로 탄소나노트브실의 강도를 예측하는 것을 목표로 한다.

먼저 구조적 유사성에 근거하여 기존에 많이 연구되어 왔던 스테이플 실의 이론들을 활용하여 탄소나노튜브실의 인장 강도를 예측하였다. 이론 값과 실험 값을 비교하여 탄소나노튜브실을 기존 이론에 적용함에 있어 문제점 및 보완되어야 할 부분에 대해 분석하였다.

외부 응력에 대한 탄소나노튜브실의 기계적 거동을 현장 편광 라만 분광법을 사용하여 내부구조 변화를 관찰하여 조사하였다. 먼저 탄소나노튜브실 내부 탄소나노튜브의 섬유배향함수를 편광 방향과 실의 축간의 상대적인 강도에 따른 편광강도 차이로부터 결정하였으며 동시에 내부 탄소나노튜브의 기계적 변형을 라만 밴드의 이동으로부터 관찰하였다. 기존의 스테이플 실의 이론과 더불어 탄소나노튜브실의 인장 및 비틀림 거동을 변형에 따른 내부 탄소나노튜브의 움직임 및 변형에 초점을 맞추어 분석하였다.

탄소나노튜브실의 인장강도를 예측하는 새로운 모델을 내부구조 변화에 근거하여 개발하였다. 새로운 모델을 만들기 위해 탄소나노튜브실의 현장 인장실험을 수행하고 탄소나노튜브실의 단면을 밀링하여 외부 응력에 따른 내부구조의 변화를 관찰하였다. 실험 결

과를 통해 실의 판단을 일으키는 주요 메커니즘이 내부 탄소나노튜브 간 미끌림 현상에 의거함을 밝혔다. 반 데르 발스 힘과 실 고유의 구조에 따른 측압에 따른 계면 전단 응력을 인장 강도로 정의하는 모델을 설계하였다. 탄소나노튜브실 내부의 탄소나노튜브의 단위를 정의하는 육방최밀충전 구조를 가지는 탄소나노튜브 클러스터라는 새로운 개념을 도입하였다. 탄소나노튜브 클러스터 간 계면 전단 응력에 의해 예측된 인장 강도는 실험 결과값을 예측하는데 적합함을 입증하였다.

마지막으로 탄소나노튜브실의 인장 강도를 향상시키기 위한 전략을 제시하였다.

핵심어: 탄소나노튜브실, 인장 강도, 기계적 거동, 라만분광법, 분자동역학, 계면전단응력

학번: 2008-20679

감사의 글

배움에 대한 열망으로 관악에 온지 벌써 10여년의 시간이 흘렀습니다. 길고도 길었던 학부 그리고 대학원 생활이 어느덧 마무리를 향해 간다고 생각하니 많은 아쉬움이 남으면서도 아직 실감이 나지 않습니다. 대학원 생활 동안, 즐거운 시간도 있었고 때론 힘들기도 했지만 연구실 생활을 하면서 배운 경험들은 저에게 있어 세상 무엇과도 바꿀 수 없는 소중한 자산으로 평생 남을 것 입니다.

먼저 이 논문이 있기까지 아직까지도 많이 부족한 저를 격려해주시고 조언해주신 유웅렬 교수님께 감사의 말씀을 드리고 싶습니다. 많은 관심과 애정을 가져주시고 항상 믿어주시고 보살펴주셔서 진심으로 감사 드립니다. 때론 교수님 기대에 부응하지 못하여 실망을 시켜드릴 때도 많았지만 앞으로는 좀 더 나은 모습을 보이는 제자가 될 수 있도록 노력하겠습니다. 바쁘신 와중에 시간을 내어주시고 논문 심사를 해주신 윤재륜 교수님, 정관수 교수님, 정영진 교수님 그리고 김민선 박사님께도 감사 드립니다.

짧게는 몇 개월 길게는 6년이 넘게 동고동락해온 연구실 식구들에게도 감사의 말씀을 드립니다. 처음 연구실에 들어와서 적응을 잘 못하던 시기에 친절하게 대해준 경주, 결혼하고 나서는 자주 못 보지만, 함께 공부하며 고생했던 것들 좋은 추억으로 남게 해줘서 고맙다. 석진이 형은 텍사스에서 잘 지내시는지 궁금합니다. 공부를 진정으로 즐기고 항상 연구에 몰두하는 형의 모습은 처음 연구실 생활을 시작하는 저에게 큰 귀감이 되었습니다. 나를 이 연구실로 이끈 병선이, 나의 인생을 새롭게 해준 친구였고 너 덕분에 이렇게 좋은 사람들 만나고 좋은 추억거리 많이 가지고 졸업하게 되는 것 같아. 성격상 말로 잘 표현하지 못하지만 항상 고마웠다. 우리 연구실 물리의 신 해동이형, 형의 박학다식함을 언제 따라잡을 수 있을지 모르겠지만 모르는 것이 있으면 항상 형을 찾게 되었고 그때마다 친절히 알려주셔서 진심으로 감사 드립니다. 그리고

나와 정반대의 성격을 지닌 내 동기 현철이, 너가 없었으면 대학원 생활을 내가 어떻게 견디고 버텨냈을지 상상이 안되. 항상 의지만 하고 도움은 별로 주지 못한 것 같아 미안한 마음도 있고 정말 고마워. 앞으로 우리 실험실을 이끌어갈 차기 방장 원진이. 요새 일 많이 하고 여러모로 많이 도와줘서 고마워. 힘든 내색하지 않고 잘 도와주고 따라와줘서 너무 고맙다. 실험실 유일한 동갑내기 친구 규민이 항상 유쾌한 분위기로 연구실을 즐겁게 해줘서 고마웠다. 앞으로 더욱 열심히 해서 좋은 결과가 있기를 진심으로 바래. 연구실 귀염둥이 태형이, 박사 수료 후 연구에 대해 많은 스트레스를 받기도 하지만 넌 영특하니까 잘 해낼 거라 믿는다. 가까운 미래에 후배들을 다독이며 연구실을 잘 이끌어가 주길 바란다. 이번에 졸업을 같이 준비하며 많이 의지했던 근성이, 10월달 상하이 학회 때부터 우리 둘 다 서로 정말 고생 많았지. 정말 나중에 우리 둘 모두 성공해서 보상받는 날이 올 거라고 믿어. 앞으로도 열심히 하자. 많이 괴롭히기도 하고 장난치기도 했던 호성이, 깐족거리면서도 연구에 대해서는 항상 진지하고 열정이 넘치는 너의 모습을 보며 자극을 받을 때도 많이 있었던 것 같아. 나중에 꼭 좋은 연구자가 되어 같이 일했으면 좋겠다. 실험실의 홍일점 사랑이, 연구실에서 혼자 여자라 힘들고 불편한 점도 많을 텐데 그래도 밝게 잘 적응해 나가는 모습이 기특할 때가 많았어. 너 역시 머리가 좋으니까 대학원 생활 앞으로도 잘 해낼 거라고 믿는다. 석빈이는 항상 알아서 잘하니까 크게 걱정되는 게 없구나. 너답게 긍정적으로 해온 대로만 하면 좋은 결과 있을 거야. 저녁에 밥 시켜 먹을 때 항상 든든하게 내편이 되어 줘서 고마웠다. 최근에 가장 일을 같이 많이 하게 된 유빈이, 부족한 나를 잘 따라줘서 진심으로 고맙다. 너가 없는 지금의 나는 상상하고 싶지도 않구나. 앞으로도 같이 열심히 해서 좋은 결과 내자. 그리고 예전에 말했던 것처럼 언젠가 우리 나라를 선도할 훌륭한 연구자가 되도록 하자. 금연하고 싶을 때 나의 금연의지를 가볍게 꺾어 주었던 성진이, 굳은 일도 군말 없이 항상 열심히 해줘서 너무 고맙다. 성격도 좋고 애기가 잘 통해서 같이

있는 시간이 정말 즐거웠던 것 같아. 짧은 시간에 많이 가까워진 민창이, 요새 많이 아프던데 앞으로도 연구실 생활 잘할 수 있을지 걱정이 많이 된다. 아픈 거 빨리 털어내고 건강한 모습으로 연구실에서 볼 수 있으면 정말 좋을 것 같아. 연구실 막내 원보, 갑자기 나랑 일하게 되어 피곤한 일도 힘든 일도 많았을 텐데 잘 따라줘서 고맙고 앞으로도 더욱 열심히 하자.

일년에 자주 못 보지만 마음 속으로 항상 생각하게 되는 고등학교 친구들 효성이, 현태, 정택이, 제호, 제원이 다들 어느새 어른이 되어 결혼도 하고 세월이 정말 빠른 것 같아. 바쁘다는 핑계로 소홀했었는데 모두 항상 행복하고 건강하길 바란다.

같이 알고 지낸 지도 어언 10년이 되가는 학부 동기들, 조세, 지훈이, 석준이, 진욱이, 규정이, 성묵이, 유용이, 승현이 지금은 각자 다른 길을 가고 있지만 나중에 다들 성공해서 즐거운 마음으로 만났으면 좋겠다. 각자의 분야에서 꼭 성공하도록 열심히 노력하자.
너무 많아 일일이 언급하기 힘들지만 힘든 학위과정을 함께 거친 재료공학부 동기들에게도 감사함과 축하를 보냅니다.

끝으로 사랑하는 가족에게 진심으로 감사를 전하고 싶습니다. 부족한 아들이지만 항상 사랑으로 보살펴 주신 부모님 감사합니다. 앞으로 더욱 더 정진하여 승승장구하는 아들이 되도록 노력하겠습니다. 말로는 표현 못했지만 누나, 여동생 민영이 뒤에서 항상 응원해줘서 고맙고 매번 집에 늦게 들어와서 자주 인사도 못 드리지만 항상 따뜻하게 맞아 주시는 할머니 감사합니다.

일일이 언급하지 못했지만 제게 많은 도움을 주시고 사랑을 주신 모든 분들께 감사 드립니다.